The Atr-Chek1 pathway inhibits axon regeneration in response to Piezo-dependent mechanosensation

Feng Li[1,2,10], Tsz Y. Lo[1,10], Leann Miles[3,10], Qin Wang[1,2,10], Dan Li[1], Jingwen Niu[4], Jessica I Goldshteyn[1], Chuxi Wang[1], Shuchao Wang[1], Jingyun Qiu[1], Shannon Trombley[1], Katarzyna Pogoda[5,6], Megan Brewster[7], Panteleimon Rompolas[7], Ye He[8], Paul A. Janmey[5], Gareth M. Thomas[4,9], Yuanquan Song[1,2*]

[1]Raymond G. Perelman Center for Cellular and Molecular Therapeutics, The Children's Hospital of Philadelphia, Philadelphia, PA 19104, USA

[2]Department of Pathology and Laboratory Medicine, University of Pennsylvania, Philadelphia, PA 19104, USA

[3]The Graduate Group in Biochemistry and Molecular Biophysics, University of Pennsylvania, Philadelphia, PA 19104, USA

[4]Shriners Hospitals Pediatric Research Center (Center for Neurorehabilitation and Neural Repair), Temple University School of Medicine, Philadelphia, PA 19140, USA

[5]Institute for Medicine and Engineering, University of Pennsylvania, Philadelphia, PA 19104, USA

[6]Institute of Nuclear Physics, Polish Academy of Sciences, PL-31342, Krakow, Poland

[7]Department of Dermatology, University of Pennsylvania, Philadelphia, PA 19104, USA

[8]The City University of New York, Graduate Center - Advanced Science Research Center, Neuroscience Initiative, New York, NY 10031, USA

[9]Department of Anatomy and Cell Biology, Temple University School of Medicine, Philadelphia, PA 19140, USA

[10]These authors contributed equally to this work

*Correspondence: songy2@email.chop.edu

ABSTRACT

Atr is a serine/threonine kinase, known to sense single-stranded DNA breaks and activate the DNA damage checkpoint by phosphorylating Chek1, which inhibits Cdc25, causing cell cycle arrest. This pathway has not been implicated in neuroregeneration. We show that in *Drosophila* sensory neurons, removing Atr or Chek1, or overexpressing Cdc25 promotes regeneration, whereas Atr or Chek1 overexpression, or Cdc25 knockdown impedes regeneration. Inhibiting the Atr-associated checkpoint complex in neurons promotes regeneration and improves synapse/behavioral recovery after CNS injury. Independent of DNA damage, Atr responds to the mechanical stimulus elicited during regeneration, via the mechanosensitive ion channel Piezo and its downstream NO signaling. Sensory neuron-specific knockout of Atr in adult mice, or pharmacological inhibition of Atr-Chek1 in mammalian neurons *in vitro* and in flies *in vivo* enhance regeneration. Our findings reveal the Piezo-Atr-Chek1-Cdc25 axis as an evolutionarily conserved inhibitory mechanism for regeneration, and identify potential therapeutic targets for treating nervous system trauma.

INTRODUCTION

Axon regeneration in the adult central nervous system (CNS) is rather limited, due to the diminished regenerative potential of mature neurons and the inhibitory microenvironment[1-4]. As a result, permanent disability often occurs in individuals with spinal cord injury or stroke. By contrast, neurons in the peripheral nervous system (PNS) are generally capable of robust axon

regeneration and regain functional recovery after injury. However, in cases of severe peripheral nerve insults, such as proximal nerve lesions or complete transections, neurological deficits can still occur due to the slow rate of spontaneous axon regeneration, failure of reinnervation or the development of chronic pain[5]. In humans particularly, minimal clinically meaningful restoration of motor function has been observed[6-8]. Moreover, the regenerative capacity of the PNS declines with aging[9]. Therefore, strategies need to be developed to increase the rate and/or extent of axon regeneration to improve functional outcomes in the adult mammalian CNS and PNS.

To achieve this goal, a major focus of research is to identify the neuronal intrinsic molecular machinery that triggers the regenerative response or acts as a regeneration brake. Various injury paradigms in different model organisms have been established[10] that serve as screening platforms. We previously developed a *Drosophila* peripheral sensory neuron injury model that displays neuronal type-specific regeneration: class IV but not class III dendritic arborization (da) sensory neurons are able to regenerate[11]. Utilizing this tool, we have performed genetic screens and identified the RNA processing enzyme Rtca as an evolutionarily conserved inhibitor of axon regeneration, which links axon injury to ER stress and RNA modifications[12]. We have thus performed an additional screen on other cellular stress pathways focusing on the DNA damage response (DDR). We found that mediators of the DNA single-strand break (SSB) response specifically inhibit axon regeneration.

SSBs are known to activate Atr (ataxia telangiectasia and Rad3 related), a serine/threonine kinase that directly phosphorylates Chek1 (checkpoint kinase-1). Chek1 in turn phosphorylates and inhibits the phosphatase Cdc25C (cell division cycle 25C) or Cdc25A, which would prevent Cdk1(cyclin-dependent kinase 1)/CycB (cyclin B) from being dephosphorylated and therefore cause a cell cycle arrest in G2/M or S-phase, respectively[13, 14]. A multistep model

has been proposed for Atr checkpoint activation in response to DNA damage[15], which involves DNA damage sensing, signal transduction and execution. DNA damage generates ssDNA (single-stranded DNA), which is recognized and coated by RPA (Replication protein A). The primed ssDNA recruits Atr-Atrip (Atr interacting protein) and facilitates the loading of 9-1-1 (Rad9-Hus1-Rad1) by the Rad17 complex. The 9-1-1 complex may then stimulate the kinase activity of Atr-Atrip, leading to phosphorylation of its substrates including Rad17 and Rad9. Phosphorylated Rad17 and Rad9 may facilitate the recruitment of downstream signaling proteins Claspin and TopBP1 (topoisomerase (DNA) II binding protein 1), allowing them to be efficiently phosphorylated by Atr. Phosphorylated TopBP1 may further stimulate the kinase activity of Atr, whereas phosphorylation of Claspin may promote the phosphorylation and activation of Chek1.

Atr can also be activated by mechanical force. It has been reported that Atr can respond to mechanical stimuli, such as osmotic stress, in mediating chromosome dynamics, which is independent of DNA damage[16]. However, the underlying mechanoreceptor remains unknown. We have recently demonstrated that the mechanosensitive (MS) ion channel Piezo is activated during axon regrowth, leading to local elevation of calcium transients and the activation of the Nos (nitric oxide synthase) cascade to restrict axon regrowth, and that Piezo loss of function (LOF) promotes class III da neuron axon regeneration[17]. The downstream cellular and molecular signaling of Piezo-Nos, however, remains elusive. Moreover, mammalian Piezo1 can be activated by osmotic stress[18] and also functions as a regeneration inhibitor[17]. Here we show that Atr-Chek1 and the associated checkpoint complex act downstream of Piezo to suppress axon regeneration by inactivating Cdc25-Cdk1. Instead of sensing DNA damage, Atr responds to the mechanical stress elicited after axon injury, with Piezo as the mechanosensor and NO (nitric oxide) as the mediator. We further show that blocking Atr-Chek1 promotes axon regeneration

both in the PNS and CNS, leading to synapse regeneration and behavioral recovery. The function of Atr-Chek1 in inhibiting axon regeneration appears to be evolutionarily conserved in mammals. This study identifies an unexpected role of the Atr-Chek1 kinase cascade in regulating neuroregeneration, reveals a mechanistic link to the mechanosensitive ion channel Piezo, and provides potential therapeutic targets for stimulating nerve repair.

RESULTS

Atr-Chek1-Cdc25-Cdk1 regulate axon regeneration

We used the previously described *Drosophila* da sensory neuron injury model[11, 12] to study axon regeneration. In brief, using a two-photon laser, we injured the axon of the mechanosensitive class III da neurons (labeled with *19-12-Gal4>CD4tdGFP, repo-Gal80*) in the PNS of early 3rd instar larvae. Degeneration of the distal axon was confirmed at around 24 hours after injury (h AI) and regeneration was assessed at around 72 h AI (Fig. 1a). In contrast to wild-type (WT) class III da neurons which failed to regenerate (Fig. 1a, arrow), in a null mutant[19] of the *Drosophila* homologue of Atr – *meiotic 41/mei41*^{29D}, new axons regrew substantially beyond the injury site (Fig. 1a, arrowheads). The function of Atr/mei41 is cell-autonomous because its RNAi knockdown in class III da neurons (*19-12-Gal4>mei41 RNAiv103624*) recapitulated the enhancement of regeneration. As expected, class III da neuron specific RNAi knockdown of the fly homologue of Chek1 – grapes/grp (*19-12-Gal4>grp RNAiBL27277* and *19-12-Gal4>grp RNAiv10076*), or *grp*^{A196} mutant clones of class III da neurons (using MARCM[20]) also enhanced axon regeneration, similarly to Atr/mei41 deficiency (Fig. 1a, arrowheads). On the other hand, class III da neuron specific overexpression of twine/twe or string/stg (*19-12-Gal4>twe* or *19-12-Gal4>stg*), the fly homologues of Cdc25C/Cdc25A which are negatively regulated by Chek1,

promoted axon regeneration (Fig. 1a, arrowheads). Cdc25 is known to activate Cdk1 by removing the inhibitory phosphorylation at tyrosine 15 (Y15) and the adjacent threonine (T14) residues[14]. We therefore overexpressed the phospho-acceptor mutant of Cdk1 – Cdk1.T14A.Y15F, which renders it unable to be phosphorylated and is thus the activated form[21], in class III da neurons (*19-12-Gal4> Cdk1.T14A.Y15F*). We found that it was sufficient to trigger axon regeneration (Fig. 1a, arrowheads). Moreover, knocking down Cdc25/twe in class III da neurons in the *mei41*^{29D} background abolished the enhanced regeneration phenotype (Fig. 1a, arrow), consistent with a model in which Cdc25/twe lies downstream of Atr/mei41 to regulate axon regeneration. The regeneration phenotype was further quantified by assessing the "Regeneration percentage" and "Regeneration index" (Fig. 1b, c, Supplementary Fig. 1a and Methods), as described previously[11]. We also quantified class III da neuron dendrite branching after blocking the Atr pathway and did not observe obvious change in total dendrite length (Supplementary Fig. 1b), suggesting a specific role of this pathway in axon regeneration.

Conversely, we determined whether gain of function (GOF) of Atr-Chek1 would reduce the regenerative potential of class IV da neurons, which are normally capable of regeneration[11]. We labeled class IV da neurons with *ppk-CD4tdGFP* and used the following injury paradigm: axotomy was induced at 3rd instar, degeneration was confirmed at 24 h AI and regeneration was assayed at 48 h AI[12]. Compared to WT class IV da neurons, which exhibited axon regeneration about 80% of the time (Fig. 1d-f, arrowheads), overexpression of wild-type human ATR (hATR-WT) in class IV da neurons significantly reduced the axon regeneration percentage to 50% and decreased the length of the regrown axons (Fig. 1d-f, arrows). However, its kinase dead version (hATR-KD) did not significantly alter regeneration (Fig. 1d-f, arrowheads), indicating that the kinase activity of Atr is required for regeneration inhibition. Consistent with this finding,

overexpression of Chek1/grp or human CHEK1 (hCHEK1) also led to reduced class IV da neuron axon regeneration (Fig. 1d-f, arrows). The fact that human ATR and CHEK1 are both capable of inhibiting axon regeneration in flies suggests that the role of Atr-Chek1 in mediating regeneration may be evolutionarily conserved. This was further confirmed by analyzing their role in mammalian axon regeneration (see below). Moreover, RNAi knockdown of Cdc25/twe in class IV da neurons, or LOF of Cdk1[22, 23] as in transheterozygotes of *Cdk1*$^{B47/E1-23}$ impeded axon regeneration to a similar extent (Fig. 1d-f, arrows). Lastly, hATR-WT failed to inhibit axon regeneration when co-expressed with the constitutively active Cdk1 (T14A, Y15F) (Fig. 1d-f), confirming that Cdk1 functions downstream of Atr in regulating axon regeneration. Together, these LOF and GOF analyses demonstrate that the Atr-Chek1 cascade modulates neuroregeneration, with Atr/mei41-Chek1/grp and Cdc25/twe-Cdk1 functioning as anti- and pro-regeneration factors, respectively.

We next examined the expression pattern of Atr/mei41 using a transgenic fly that contains a fosmid clone of the FLAG tagged mei41 genomic locus – mei41::FLAG, so that FLAG expression reflects the endogenous pattern of mei41 at the physiological level[24]. We found that mei41::FLAG is present in class III da neurons, restricted within the nucleus (Supplementary Fig. 1c, red dashed circle). We did not detect obvious differences in the expression level or distribution of mei41::FLAG between uninjured and injured class III da neurons at 24 or 48 h AI (Supplementary Fig. 1c). The expression of mei41::FLAG was also found in other types of da neurons, including class IV da neurons (Supplementary Fig. 1c, yellow dashed circle), suggesting that Atr/mei41 *per se* is likely not a determining factor for the regeneration cell type specificity.

To determine the specificity of the Atr-Chek1 pathway in regulating regeneration, we

queried the other classical DDR branch which is triggered by double-strand DNA breaks (DSB). Once DSBs are generated, Atm (ataxia telangiectasia mutated) is recruited by the Mre11-Rad50-Nbs1 (MRN) complex to sites of broken DNA and phosphorylates downstream substrates such as Chek2 (checkpoint kinase 2)[13]. The fly homologues of Atm, Rad50 and Nbs are telomere fusion/tefu, rad50 and nbs1, respectively. We found that their LOF mutations, as in *tefu*$^{atm-6}$ [25], *rad50*^{EP1} [26] and *nbs*^{1} [27] did not result in significant defects in class IV da neuron axon regeneration (Supplementary Fig. 2a, b). Furthermore, LOF of Atm/tefu as in *tefu*$^{atm-6/atm-3}$ [25] did not lead to enhanced axon regeneration in class III da neurons (Supplementary Fig. 2c-e, arrow). These observations highlight the unique role of the Atr-Chek1 pathway in mediating neuroregeneration and also raise the question whether DNA damage is indeed involved. Moreover, we examined the axon regeneration phenotype in the regeneration-incompetent class I da neurons[11] and found that *Atr/mei41* mutants also showed increased regeneration (Supplementary Fig. 2f-h, arrowheads). This suggests that the regeneration-inhibition function of the Atr pathway is applicable to multiple neuronal cell types, as is further exemplified by our regeneration studies in mammals (see below).

Atr-Chek1 inhibits axon regeneration independent of DNA damage

In the DDR, ssDNAs induced by DNA damage are sensed by RPAs, which then recruit and activate Atr, orchestrated by additional factors. The imminent question is whether DNA damage is implicated in Atr activation during neuroregeneration. To address this question, we first assessed whether DNA damage is induced after axon injury in class III da neurons. γH2AX (H2A histone family, member X) – the serine 139 phosphorylated form of H2AX serves as the gold standard DNA damage marker[28, 29]. Its fly homologue is His2Av and a phospho-specific

antibody against His2Av – p-His2Av has been widely used for detecting DNA damage in flies[30]. Using this antibody, we found there was no difference, in terms of p-His2Av staining, between injured and uninjured class III da neurons at 5 min, 24 h or 48 h AI (Fig. 2a, dashed circles), suggesting that DNA damage is not significantly induced after axon injury or during axon regeneration in da sensory neurons. Second, we tested whether His2Av LOF affects axon regeneration and found that class III da neuron specific knockdown of His2Av with a previously reported RNAi[31] did not increase axon regeneration (Fig. 2b-d, arrow). Third, we asked whether blocking the ssDNA sensing step by eliminating RPAs would interfere with Atr's function in regeneration. RPA is a heterotrimer composed of three subunits Rpa1, Rpa2 and Rpa3. Therefore, we expressed in class III da neurons RNAis targeting their fly homologues RpA-70, RPA2 and RPA3 and found no enhancement of axon regeneration (Fig. 2b-d, arrow). This was further confirmed by the *RPA2*^{KG00759} amorphic mutant[32] class III da neurons (using MARCM) and the *RPA3*^{G0241} LOF allele[33] (Fig. 2b-d, arrow). Lastly, overexpression of RpA-70, RPA2 or RPA3 in class IV da neurons did not reduce their axon regeneration (Supplementary Fig. 3a, b). These data strongly suggest that the neuronal intrinsic DDR does not contribute significantly to injury-induced axon regeneration in da sensory neurons, and that the Atr-Chek1 pathway inhibits axon regeneration independent of DNA damage.

The Atr-associated checkpoint complex inhibits axon regeneration

The RPA-mediated DNA damage sensing step is thus dispensable for Atr's inhibition of axon regeneration. However, we wondered whether other factors in the checkpoint complex, which are important for the signal transduction and execution steps, facilitate the regulation of regeneration. We focused on Atrip, Rad17, the 9-1-1 complex composed of Rad9-Hus1-Rad1,

TopBP1 and Claspin (Fig. 3b). We found that class III da neuron specific RNAi knockdown targeting their fly homologues Atrip/mus304, Rad17, Rad1, TopBP1/mus101 and Claspin all markedly increased axon regeneration (Fig. 3a, c, d, arrowheads). The regeneration enhancement phenotype via TopBP1/mus101 RNAi knockdown was recapitulated in a LOF mutation – *mus101*^{A} (Fig. 3a, c, d, arrowheads). Moreover, LOF of Hus1-like, the fly homologue of Hus1, in an insertional allele *Hus1-like*^{MI11259} which abolished its expression (Supplementary Fig. 4b, c), also promoted axon regeneration (Fig. 3a, c, d, arrowheads). Because the Hus1-like insertion was also mapped to the promoter region of a neighboring gene – *ctrip* (Supplementary Fig. 4a), we thus analyzed an insertional mutant of *ctrip* – *ctrip*^{MI14762}, but did not observe a regeneration phenotype in class III da neurons (Supplementary Fig. 4d). These data indicate that the checkpoint complex known to be required for transducing the DNA damage signal is also essential for facilitating Atr-Chek1 to cell autonomously inhibit neuroregeneration.

In order to further assess the involvement of the Atr-Chek1 pathway members in sensory neuron regeneration, we determined the expression pattern of the relevant molecules we analyzed in *Drosophila* and mammals. First, we examined expression of Cdc25/twe in da neurons with antibody[34] staining and found it was present in both uninjured and injured class III da neurons, similar to Atr/mei41 (Supplementary Fig. 5a). Second, we performed immunostaining for Atrip, Chek1 and TopBP1 using mouse dorsal root ganglion (DRG) tissues, and found that each of these proteins was expressed with/without sciatic nerve lesion (SNL) (Supplementary Fig. 5b). Third, as extensive gene expression analyses had been performed in mouse and human DRGs, we thus queried the transcript level of Atr-Chek1 pathway members in a number of these databases[35, 36], and found that they were all expressed in the mouse or human DRG, although at a low to medium level (Supplementary Fig. 5c). This is consistent with a

potential homeostatic function of this pathway in non-dividing cells.

Blocking the Atr-Chek1 pathway promotes behavioral recovery and synapse regeneration

Initiation of axonal regrowth is only the first step towards repairing lost connections. True repair requires that regenerating axons find their targets and reform functional synapses. In general, this process of functional regeneration is poorly studied in the field. To our knowledge, this has never been documented in any *Drosophila* injury models[37]. To assess functional recovery in flies, we utilized a behavioral paradigm based on the larval gentle-touch response[38] – gently touching larval anterior segments (thoracic (T) segments and the first abdominal segment) with an eyelash elicits a set of stereotypical responses that are readily quantifiable (Supplementary Fig. 6b). We further subcategorized the intensity of the gentle-touch stimulus based on the contact area between the eyelash and the body segment: touch+, touch++ and touch+++, with the eyelash diameter covering <1/8, 1/8-1/4 or 1/4-1/2 of the segment, respectively (Supplementary Fig. 6a). Larvae showed a graded response according to the stimulation intensity (Fig. 4c, e, g and Supplementary Fig. 6d-f). As shown previously, the mechanosensitive class III da neurons mediate gentle-touch sensation[39]. We further found that there is a segment-wise somatosensory map for gentle-touch: class III da neuron axons project into the VNC (ventral nerve cord) in an anterior-posterior pattern, that is, axons from the T1 segment constitute the anterior-most T1 bundle within the VNC (Fig. 4a), and that injuring the class III da neuron axon bundle at T1 or T2 in the VNC (Fig. 4a) led to an impaired touch response specifically at segment T1 or T2, without affecting neighboring segments (Supplementary Fig. 6c).

Given this precision, we injured class III da neuron axons at the T1 & T2 bundles in the VNC, then specifically stimulated the T1, T2, T3 or A1 (abdominal) segment, and scored the

touch response at 8, 24 and 48 h AI. We found that in WT control, axon injury in the VNC resulted in failed gentle-touch response at the T1 & T2 segments without affecting the T3 & A1 segments, when tested at 8 h AI (Fig. 4c, e, g and Supplementary Fig. 6d-f, Supplementary Video 1). This defect persisted at 48 h AI (Fig. 4c, e, g and Supplementary Video 2), with 0% and 7.3% of the larvae displayed behavioral recovery at 24 and 48 h AI (Fig. 4b, d, f and Methods), respectively. We went on to assess the behavioral outcome after inhibiting the Atr-Chek1 pathway focusing on mei41, Rad17 and mus101, all of which showed strong axon regeneration phenotype. Strikingly, after knocking down *Rad17* in class III da neurons, in $mei41^{29D}$ mutants and in particular in the *mus101* mutant – $mus101^{A}$, we observed substantial behavioral recovery as early as 24 h AI (26%), which continued to improve at 48 h AI (43.5%) (Fig. 4b, d, f and Supplementary Videos 3-6). The response score was also statistically improved with the touch+++ stimulation (Fig. 4c, e, g). In the meantime, the behavioral response in the uninjured T3 and A1 segments were comparable among the different genotypes (Supplementary Fig. 6d-f). These results demonstrate that inhibiting the Atr-Chek1 pathway is not only beneficial for axon regrowth, but also promotes functional regeneration.

In order to assess synapse regeneration, we first sought to confirm that class III da neurons form cholinergic synapses in the CNS. We found that class III da neurons were co-labeled by *nompC-QF>mCD8GFP* (the class III da neuron marker) and *ChAT-Gal4>CD4TdTomato* (Supplementary Fig. 6g), which marks essentially all cholinergic neurons[40]. We used synaptotagmin-GFP (syt.eGFP/syt)[41] to mark class III da neuron presynapses (Fig. 5b), which were tightly opposed by postsynaptic cholinergic receptors labeled by α-bungarotoxin (α-BTX)[42] (Fig. 5a). We then ablated the class III da neuron axon bundles on one side of the VNC, which retracted out of the neuropil within 8 h AI (Fig. 5c). At 24 h AI, WT

277 axons rarely regrew into the neuropil, displaying retraction bulb like structures (Fig. 5c). We
278 subsequently focused on the *mus101*^{A} mutants, as they demonstrated most robust behavioral
279 recovery. In contrast to WT, *mus101*^{A} mutant class III da neurons not only exhibited extensive
280 axon regeneration (~50%) back into the neuropil, but also increased the percent of regenerating
281 axons containing syt puncta, indicative of synapse reformation (Fig. 5c, d, arrowheads).
282
283 **Atr functions downstream of Piezo and Nos in regulating axon regeneration**
284 Since Atr is not activated by DNA damage during neuroregeneration, what, then, is the trigger?
285 We speculated that mechanical stimulus may be the culprit, based on several lines of evidence.
286 First, mechanical stress such as osmotic stress is capable of relocating and activating Atr, which
287 then phosphorylates Chek1[16]. Second, during axon regeneration, mechanical force is reported to
288 stimulate the MS ion channel Piezo, leading to local calcium elevation in the growth cone and a
289 signaling cascade mediated by Nos to inhibit regeneration[17]. Third, removal of Piezo or Nos
290 promotes class III da neuron axon regeneration to a similar extent as Atr/mei41 LOF. Fourth, we
291 found that *PiezoKO* also increased class I da neuron axon regeneration as well as *Atr/mei41*
292 mutants (Supplementary Fig. 2f-h, arrowheads). Lastly, Piezo can be activated by osmotic
293 stress[18]. Therefore, we hypothesized that Piezo transduces the mechanical signal elicited during
294 neuroregeneration, to trigger activation of the Atr-Chek1 pathway.
295 As a first step to testing this hypothesis, we sought to determine whether Atr's response
296 to osmotic stress is Piezo-dependent. We first reproduced the hypotonic stress-induced Atr
297 relocalization/clustering phenomenon previously shown in HeLa cells[16]. Using WT HEK 293T
298 cells, we found that exogenously expressed FLAG tagged human ATR also formed clusters in
299 the nucleoli under hypotonic condition (Fig. 6a, dashed circles). However, in PIEZO1 knockout

HEK 293T cells (*PIEZO1KO*)[43], ATR clusters were much less abundant. Even if they were induced, they appeared smaller in size and showed reduced fluorescence intensity (Fig. 6a-c). We then went on to determine whether Atr clustering relies on Nos, as it is downstream of Piezo. We pharmacologically manipulated NOS, and found that inhibiting NOS with 1400W dihydrochloride[44] attenuated the ATR clustering induced by hypotonic stress, whereas activating NOS with histamine[45] rescued the reduced ATR clustering in *PIEZO1KO* (Fig. 6d-f). These results indicate that the mechanical stress-induced Atr relocalization relies on the presence of Piezo and Nos, and that Piezo can function as a mechanoreceptor underlying Atr's response to mechanical stimulus.

Second, we performed genetic interaction and epistasis analyses to determine the relationship between Atr/mei41 and the Piezo-Nos pathway. Genetic interaction analyses showed that while transheterozygotes of $mei41^{29D/+}$*; PiezoKO/+* did not show a regeneration phenotype, $mei41^{29D/+}$*;* $Nos^{\Delta 15/+}$ significantly promoted class III da neuron axon regeneration, similar to homozygous mutants of $mei41^{29D}$, *PiezoKO* or $Nos^{\Delta 15}$ (Fig. 7a-c). This result indicates that Atr/mei41 and Piezo-Nos function in the same genetic pathway, and further suggests that, although Atr/mei41 does not associate with Piezo *per se*, it appears to closely interact with Nos. Moreover, our epistasis analysis showed that: 1) class III da neuron-specific overexpression of Chek1/grp reduced the enhanced regeneration phenotype in *PiezoKO*; 2) overexpression of Chek1/grp also attenuated the regeneration enhancement in $Nos^{\Delta 15}$ mutants; 3) on the other hand, class III da neuron specific overexpression of mPiezo1-TriM, an over-activating mutant of mouse Piezo1 that reduces axon regeneration when overexpressed in class IV da neurons[17], did not significantly reduce the enhanced regeneration in $mei41^{29D}$ mutants; 4) overexpression of Nos, which inhibits axon regeneration in class IV da neurons[17], also failed to attenuate the

323 regeneration phenotype in *mei41*^{29D} mutants (Fig. 7a-c). These data collectively suggest that
324 Atr/mei41 operates downstream of Piezo-Nos and that Atr/mei41 overrides the regeneration
325 phenotype that results from removal of Piezo or Nos.

326 Third, our results that Atr/mei41 genetically interacts with Nos and that Nos activity is
327 required for the mechanical stress-induced Atr clustering suggest that Piezo feeds into the Atr-
328 Chek1 pathway through NO (nitric oxide) signaling, which would be consistent with a previous
329 finding that NO promotes p53 nuclear retention in an Atr-dependent manner[46]. To directly
330 visualize NO propagation, we performed NO imaging using the fluorescent NO dye DAF-FM
331 diacetate[47, 48]. While NO production was rarely detected in uninjured class III da neurons (Fig. 7f
332 and Supplementary Fig. 7), we observed obvious fluorescence signal around the axon tip, along
333 the axon and in the cell body, in 62.5% of the WT class III da neurons at 24 and 48 h AI (Fig. 7d,
334 f). As a negative control, we found that the signal of the NO dye was drastically reduced in the
335 Nos mutant – *Nos*$^{\Delta 15}$ (Fig. 7d, f, g). Importantly, NO production was similarly abolished in
336 *PiezoKO* (Fig. 7e-g). This result, together with the genetic analyses, suggests that NO functions
337 as a key messenger that links the activation of the Piezo channel during axon regeneration, to the
338 downstream Atr-Chek1 pathway.
339
340 **Pharmacological and genetic inhibition of the Atr-Chek1 pathway promotes axon**
341 **regeneration in mammalian neurons *in vitro* and *in vivo***
342 Having established that hATR and hCHEK1 inhibit axon regeneration in flies, we hypothesized
343 that Atr-Chek1 may also function as regeneration inhibitors in mammals. First, we tested this
344 hypothesis using an injury paradigm in cultured neurons *in vitro* based on a microfluidic device[49,
345 50]. In brief, embryonic (E18) rat DRG neurons were cultured in a microfluidic chamber that

separates the neurites from the soma. The neurites in the terminal chamber were removed by vacuum aspiration at 7 days *in vitro* (DIV7) and regeneration was assessed at various time points after injury. We tested the efficacy of Atr and Chek1 inhibitors in promoting axon regeneration. The Atr-Chek1 network is a key mediator of DDR, and inhibiting DDR has become an attractive concept in cancer therapy. To date, pharmacological inhibitors for Atr and Chek1 have already entered anti-cancer clinical trials either as stand-alone agents or combined with radio- or chemotherapy[51, 52]. We thus tested two pharmacological inhibitors of Atr – AZD6738 and VE-822 (NCT02157792, NCT02223923 and NCT02264678) and the Chek1 inhibitor MK-8776[53, 54] (NCT01870596). We found that inhibiting Atr with AZD6738 or VE-822, or inhibiting Chek1 with MK-8776 all modestly promoted axon regeneration at 18 h AI (Fig. 8a). Regrown neurite coverage areas (Methods) were modestly but significantly increased in drug-treated neurons, as compared to the vehicle-treated controls (Fig. 8b). The AZD6738-dependent neurite regrowth enhancement was already apparent at 5 h AI (Fig 8c). We next asked whether Chek1 inhibition might promote regeneration *in vivo*. To address this question, we injected the Chek1 inhibitor MK-8776 directly into fly larvae immediately after axonal injury and found that this compound significantly increased class III da neuron axon regeneration (Fig. 8d-f, arrowheads), compared to the vehicle control (Fig. 8d-f, arrow).

Third, to analyze axon regeneration in mammals *in vivo*, we utilized the sciatic nerve lesion (SNL) model in adult mice. To generate sensory neuron-specific Atr conditional knockout (*Atr cKO*), we bred mice with *Advillin-CreER; Atr*$^{fl/fl}$ alleles and induced Cre mediated recombination with tamoxifen (TAM) injection (Methods). Regenerating sensory axons were identified by SCG10 immunostaining[55] (Fig. 8g). We found that the extension of SCG10^{+} axons was significantly increased (~60%) in *Atr cKO* compared to control animals at SNL Day 3 (Fig.

8g, h). To summarize, these results suggest that the Atr-Chek1 pathway also functions intrinsically in neurons to inhibit axon regeneration in mammals, a process that may be evolutionarily conserved, and that the anti-cancer drugs targeting Atr-Chek1 may be repurposed for treating neural injury.

Piezo exerts greater inhibition of axon regeneration on soft versus stiff substrates

To begin to understand how Piezo gets activated during axon regeneration, we determined how substrate stiffness affects axon growth/regrowth in the presence or absence of Piezo1, to get an estimate of the range of force leading to Piezo1 activation. Specifically, we investigated whether the presence of Piezo1 influences how DRG neurons respond to their environment by analyzing neuronal total neurite length on the respective gel substrate that they were cultured on. To generate sensory neuron specific Piezo1 conditional knockout (*Piezo1 cKO*), we bred mice with *Advillin-CreER; Piezo1*$^{fl/fl}$ alleles and induced Cre mediated recombination with TAM injection (Methods). Adult DRG neurons were dissociated and cultured onto polyacrylamide (PAA) hydrogels of 1.0 and 30.0 kPa (1,000 and 30,000 Pa) stiffnesses[56, 57] for 38-40 hours. These stiffnesses were chosen because DRG neurons were previously reported to exhibit increased traction force at intermediate (1 kPa) to high (5 kPa) stiffnesses[58]. Meanwhile, the "extreme" stiffness (30.0 kPa), we hypothesized, would likely negate Piezo-mediated difference in traction force, since DRG neurons produce no more than an average of 50 Pa stress[58], and the fluctuation of stress that occur during extension are no more than a factor of 2 or 3[59]. Indeed, we found that there was no difference in total neurite growth between control and *Piezo1 cKO* groups when grown on 30 kPa hydrogels (Fig. 8i, j). However, on 1.0 kPa hydrogels, *Piezo1 cKO* DRG neurons exhibited significantly more total neurite length than control neurons (Fig. 8i, j),

suggesting that Piezo1 is likely to be activated on softer substrates. Worth mentioning, the elastic modulus, a measure of the tissue's resistance to deformation, ranges from 50 to 500 Pa for uninjured cortical tissues in rat, and it is even lower in injured tissues[60]. Therefore, it is possible that during axon regeneration, the local force between the axon tip and the environment falls into the range for Piezo activation. Given its enrichment at the axon tip after injury[17], these findings suggest that Piezo is thus capable of transducing the physical signals to the intracellular signaling cascades to slow down axon regeneration.

DISCUSSION

Mature neurons retain limited capacity to repair their injured nerve fibers after trauma, leading to poor functional recovery. To overcome this regeneration failure, numerous efforts have been made to increase intrinsic axon regrowth and/or remove extrinsic obstacles[1-4]. However, we still have limited understanding regarding how injured neurons integrate extrinsic information with the intrinsic signaling pathways, to make the decision to regenerate, stall, retract or die. In this study, using a *Drosophila* sensory neuron injury model, we identified the Atr-Chek1 pathway as a neuron-intrinsic negative regulator of axon regeneration. We hypothesize that during axon regeneration, the growth cone physically interacts with the environment such as the glial cells, resulting in the activation of the mechanosensitive ion channel Piezo at the growth cone tip; opening of the Piezo channels leads to local calcium influx and the activation of Nos, which then produces NO; NO functions as a second messenger and propagates to the nucleus where it activates Atr and its associated complex; Atr then phosphorylates and activates Chek1, which phosphorylates and inactivates Cdc25, inhibiting its ability to dephosphorylate and activate Cdk1; the phosphorylated and inactive Cdk1 impinges on downstream effectors, causing regeneration

failure (Supplementary Fig. 8).

The Piezo-Nos-Atr cascade thus behaves as a regeneration brake in neurons, which is capable of sensing the extrinsic cues in the local microenvironment, processes and transduces these signals to a kinase circuit originally known to respond to DNA damage, and then potentially rewires the circuit to instruct cellular events such as cytoskeleton reorganizations to curtail regeneration. Further downstream, we speculate that Cdk1 may phosphorylate multiple substrates and thus engage multiple pathways. For example, Cdk1 activates FOXO[61], and Daf16/FOXO is inhibited by the insulin/IGF1 receptor DAF-2 during age-dependent decline of axon regeneration in *C. elegans*[62]. Cdk1 also phosphorylates Nde1[63], which regulates dynein-dependent transport, another process that is important for axon regeneration[64], associating with the regulation of the cytoskeleton. Cytoskeleton dynamics, in particular microtubule and actin, have been well documented as key players in axon regeneration[65]. The Piezo-Nos-Atr machinery is not restricted to the regeneration-incompetent class III da sensory neurons in flies, as was confirmed by the presence of Atr/mei41 in other types of da neurons, and by the enhanced axon regeneration of class I da neurons in *PiezoKO* or *Atr/mei41* mutants, mammalian DRG neurons after pharmacological inhibition of Atr or Chek1, or in *Atr cKO*. We propose that this may be a mechanism adopted by injured neurons in general, as a wait-and-see strategy, allowing them the opportunity to sample the environment, assess the intrinsic status and decide whether to regenerate. Furthermore, there may be a tug-of-war in all neuronal types after injury, between factors that inhibit regeneration such as Piezo-Nos-Atr, and those that promote regeneration. In class III da neurons, because of their limited intrinsic regenerative potential, the activation of Piezo-Nos-Atr is sufficient to suppress further regeneration. However, in class IV da neurons, the endogenous regenerative drive is high enough to override this blockade. The regeneration

enhancement phenotype observed in *Atr*/*mei41* mutants is comparable to that of *PiezoKO* in flies, and both Piezo and Atr are shown to not only inhibit axon regeneration in fly larvae but also in adult sensory neurons in mice[17]. These findings raise the possibility that the Atr pathway plays an evolutionarily conserved role in regulating regeneration, which warrants further investigation.

The involvement of DNA damage in neural injury and regeneration is an emerging concept, but not well explored. p53 was reported to be required for facial nerve regeneration in mouse[66]. Whereas inhibition of Poly (ADP-ribose) polymerases (PARPs), which are involved in DNA repair, promotes axon regeneration in worms[67], no positive effect was observed in mouse[68]. An outstanding question is whether and how axon injury induces DDR. If it does, what type of DNA damage is involved? Our results, on the other hand, favor the hypothesis that DNA damage may not play a prominent role at least in fly sensory neurons after injury. However, it is worth noting that we are not able to fully rule out the involvement of DNA damage, given our lack of ability to specifically detect single-stranded DNA breaks in injured neurons. Moreover, NO itself has been reported to act as a mutagen[69]. Thus, future studies are warranted to determine the link between NO and the Atr complex, and to assess additional NO targets. Another intriguing question is whether other cell types in the microenvironment, for example the glial cells, undergo injury-induced DDR, and if so, how that may affect the regeneration outcome.

Activation of the Atr kinase is well known as the initial response to DNA damage. But interestingly, the Atr-Chek1 pathway is also involved in DNA-damage-independent functions. Mechanical stress activates Atr at the nuclear envelope to modulate chromatin dynamics and nuclear envelope plasticity[16]. Functions of the cytoplasmic Atr are associated with the centrosome, mitochondria and cytoskeleton[70]. In addition, patients with Seckel syndrome due to ATR mutations, suffer severe nervous system malfunctions including microcephaly, defective

neurodevelopment and mental retardation[71], emphasizing a crucial neural function of Atr. Our work identified the missing mechanoreceptor underlying Atr's response to mechanical stimuli, which is the mechanosensitive ion channel Piezo. Together with previous work demonstrating Piezo's inhibitory role during axon regeneration, we have uncovered a route through which the mechanical force at the growth cone is sensed, encoded, and transduced to the nucleus, to elicit a signaling cascade governing cellular events such as regeneration.

While researchers have successfully regenerated mammalian nerves by targeting intrinsic or extrinsic barriers, these exciting advancements have not yet produced successful therapeutic targets for human patients. This is partly due to our incomplete understanding about the pathways controlling regeneration. Another contributing factor is our limited capabilities to induce proper axon regeneration beyond simply promoting axon regrowth, in order to achieve adequate synapse regeneration and functional recovery. We have thus established a behavioral paradigm in flies, based on the touch sensation, for assessing functional regeneration after CNS injury. It is encouraging to find that inhibiting the Atr-Chek1 pathway presented beneficial effects towards synapse regeneration and functional recovery. It is important to point out that the enhanced behavioral recovery we observed may directly result from the *bona fide* regeneration of the injured axons, although it is possible that the sprouting of uninjured axons or circuit level plasticity may also contribute. Importantly, though, the fly sensory neuron injury model offers an ideal opportunity to screen for novel regeneration regulators, dissect the underlying genetic, cellular and molecular mechanisms, and test their functional relevance.

Finally, our results showing that pharmacological inhibition of Atr or Chek1 enhanced axon regeneration in cultured mammalian neurons and in flies *in vivo* provide a strong rationale to further test the viability of this pathway as a potential target for treating neural injury.

Importantly, the fact that these pharmacological inhibitors for Atr and Chek1, which are already in clinical trials for cancer therapy, showed efficacy in promoting axon regeneration raises the possibility of repurposing these drugs for regeneration therapy. It is worth mentioning that the inhibitor induced axon regeneration *in vitro* we observed was modest, which may be due, in part, to the simplified environment in the culture dish. In the absence of non-neuronal cell types such as glial cells, which the growth cones interact with, the mechanical force induced suppression of regeneration is less prominent compared to *in vivo*.

FIGURE LEGENDS

Figure 1. The Atr/mei41-Chek1/grp pathway regulates axon regeneration in da sensory neurons in flies.

(**a**) Class III da neuron axons fail to regenerate in WT. Atr/mei41 removal as in $mei41^{29D}$ mutants or class III da neuron specific RNAi leads to increased axon regeneration. $Chek1/grp^{A196}$ mutant clones (with MARCM), class III da neuron expression of Chek1/grp RNAis, Cdc25/twe/stg, or the dephosphorylated/activated Cdk1.T14A.Y15F increases axon regeneration. Class III da neuron expression of twe RNAi suppressed the enhanced regeneration in $mei41^{29D}$ mutants. The injury site is demarcated by the dashed circle. Arrow marks axon stalling while arrowheads show the regrowing axon tips. (**b**, **c**) Quantifications of class III da neuron axon regeneration with Regeneration percentage (b) and Regeneration index (c). N = 72, 23, 30, 16, 22, 30, 36, 30, 37 and 28 neurons from 6 to 20 larvae. (**d**) Class IV da neurons robustly regenerate in WT. Class IV da neuron specific expression of hATR-WT, grp, hCHEK1, twe RNAis, or LOF of Cdk1 as in transheterozygotes of $Cdk1^{B47/E1-23}$ impedes axon regeneration, whereas the kinase dead (KD) mutant of hATR fails to show significant effect. Overexpression of hATR-WT together with the

507 constitutively active Cdk1 (T14A, Y15F) fails to inhibit axon regeneration. (**e**, **f**) Quantifications
508 of class IV da neuron axon regeneration. N = 97, 50, 25, 30, 38, 33, 28, 24 and 23 neurons from
509 6 to 18 larvae. *P < 0.05, **P < 0.01, ***P < 0.001 by Fisher's exact test (b and e), one-way
510 ANOVA followed by Holm-Sidak's test (c) or Dunn's test (f). Scale bar = 20 μm. See also
511 Supplementary Fig. 1.
512
513 **Figure 2. The Atr-Chek1 pathway regulates axon regeneration independent of DNA**
514 **damage.**
515 (**a**) The DNA damage marker, phosphorylated histone 2A gamma (p-His2Av), is not upregulated
516 in injured class III da neurons at various time points, compared to the uninjured control. The
517 dashed teal circle marks the injury site and the cell bodies are outlined with dashed white lines.
518 The obvious staining in the neighboring epithelial cell nuclei serves as the positive control for
519 the antibody. (**b**) Class III da neuron specific expression of RNAis for His2Av, RpA-70, RPA2
520 or RPA3, $RPA2^{KG00759}$ mutant clones (with MARCM) or $RPA3^{G0241}$ mutants do not significantly
521 increase axon regeneration. (**c**, **d**) Quantifications of class III da neuron axon regeneration with
522 Regeneration percentage (c) and Regeneration index (d). N = 72, 14, 15, 24, 16, 20, 25, 24, 24
523 and 20 neurons from 4 to 20 larvae. The injury site is demarcated by the dashed circle. Arrow
524 marks axon stalling. No statistical difference is detected by Fisher's exact test (b), one-way
525 ANOVA followed by Holm-Sidak's test (d). Scale bar = 20 μm. See also Supplementary Fig. 2
526 and 3.
527
528 **Figure 3. The Atr-associated checkpoint complex inhibits axon regeneration.**
529 (**a**) TopBP1/mus101 and Hus1-like mutants, $mus101^{A}$ and $Hus1\text{-}like^{MI11259}$, and class III da

neuron specific expression of Atrip/mus304 RNAis, Rad17 RNAis, Rad1 RNAis, TopBP1/mus101 RNAi or Claspin RNAis increase axon regeneration. The injury site is demarcated by the dashed circle. Arrow marks axon stalling while arrowheads show the regrowing axon tips. (**b**) The single-stranded DNA damage pathway mediated by Atr, Chek1, Cdc25 and the associated checkpoint complex. The factors marked by the red cross are tested for their potential role in axon regeneration. (**c**, **d**) Quantifications of class III da neuron axon regeneration with Regeneration percentage (c) and Regeneration index (d). N = 72, 20, 27, 24, 30, 32, 29, 24, 23, 44, 29, 23 and 37 neurons from 6 to 20 larvae. *$P < 0.05$, **$P < 0.01$, ***$P < 0.001$ by Fisher's exact test (c), one-way ANOVA followed by Dunn's test (d), two-tailed unpaired Student's t-test (d). Scale bar = 20 μm. See also Supplementary Fig. 4 and 5.

Figure 4. Inhibiting components of the Atr-associated checkpoint complex promotes behavioral recovery after CNS injury in flies.

(**a**) Class III da neuron axon projection map in the VNC and the VNC injury paradigm. There is a segment-wise somatosensory map for gentle-touch: class III da neuron axons project into the VNC in an anterior-posterior pattern. Axons from the T1 segment constitute the anterior-most T1 bundle within the VNC. The T1 and T2 axon bundles are injured by targeting the nerve bundles right before they enter the commissure region, as marked by the red dots. Gentle-touch response is then performed by stimulating the T1 or T2 segments using an eyelash. A total of four trials are scored for each genotype. PC, pseudocephalon; T, thoracic; A, abdominal. (**b**) *mus101*^{A} mutants show enhanced gentle-touch response after VNC injury, as shown by the Recovery percentage. A larva is defined as showing recovery if the scores from at least two of the four trials are 1 or above. While WT largely fail to respond even at 48 h AI, significantly more

553 *mus101*^{A} mutants show recovery as early as 24 h AI. (**c**) Gentle-touch response scores at 8, 24
554 and 48 h AI with various stimulation intensity. *Mus101*^{A} mutants display significantly higher
555 recovery especially with the T+++ stimulus. (**d**) Class III da neuron specific knockdown of
556 Rad17 mildly increases Recovery percentage at 48 h AI. (**e**) Class III da neuron specific
557 knockdown of Rad17 improves response scores at 48 h AI. (**f**) *mei41*^{29D} mutation mildly
558 increases Recovery percentage at 48 h AI. (**g**) *mei41*^{29D} mutation improves response scores at 48
559 h AI. $N = 41$ larvae for Ctrl, 23 for *mus101*^{A}, 33 for *mei41*^{29D}, 11, 26 and 26 for *Rad17 RNAi* at
560 8 h, 24 h and 48 h. $*P < 0.05$, $**P < 0.01$, $***P < 0.001$ by Fisher's exact test (b, d and f), one-
561 way ANOVA followed by Tukey's test (c, e and g). See also Supplementary Fig. 6.
562
563 **Figure 5. Inhibiting the Atr pathway promotes synapse regeneration in flies.**
564 (**a**) Class III da neurons form cholinergic synapses in the VNC. Synaptotagmin-GFP
565 (syt.eGFP/syt) marks class III da neuron presynapses, which are tightly opposed by postsynaptic
566 cholinergic receptors labeled by α-bungarotoxin (α-BTX). Scale bar = 5 μm. (**b**) In uninjured
567 class III da (C3da) neurons (marked in green), syt puncta (marked in red) are enriched at the
568 presynaptic terminals within the neuropil. Scale bar = 20 μm. (**c**) *Mus101*^{A} mutants show
569 enhanced axon regeneration and synapse reformation in the CNS. Class III da neuron axon
570 bundles on one side of the VNC are ablated (dashed circles), resulting in the retraction of axons
571 out of the neuropil within 8 h AI. At 24 h AI, WT axons rarely regrow into the neuropil,
572 displaying retraction bulb like structures. *Mus101*^{A} mutant class III da neurons not only exhibit
573 extensive axon regeneration back into the neuropil, but also increase the percent of regenerating
574 axons containing syt puncta at the terminals (arrowheads), indicative of synapse reformation.
575 Two examples of *mus101*^{A} mutants are shown. The schematic drawings depict the VNC (blue),

neuropil (pink), uninjured axons (black), retracted axons (green) and regenerating axons (red). Scale bar = 20 μm. (**d**) Quantification of axon and synapse regeneration. *N* = 34 and 35 axon bundles from 8 and 10 larvae. The percent of regenerated axons increases from 21% in WT to 47% in ^{mus101A} mutants, **P* < 0.05 by Fisher's exact test. The percent of regenerated axon containing syt puncta is also increased in in ^{mus101A} mutants. See also Supplementary Fig. 6.

Figure 6. ATR's response to osmotic stress depends on PIEZO1 and NOS.

(**a** to **c**) Hypotonic stress-induced ATR clusters in the nucleus is attenuated in PIEZO1 knockout. (a) Exogenously expressed FLAG-ATR is present in the cytoplasm in both WT and *PIEZO1KO* HEK293T cells before treatment. 5 min or 7 min hypotonic stress induces robust clustering of FLAG-ATR in the nucleus in WT cells, which is much attenuated in the *PIEZO1KO* cells. Fewer cells produce the clusters. The clusters are smaller in size, fewer in number and lower in intensity. The dashed circles outline the nucleus. Scale bar = 10 μm. (b) Quantification of the fluorescence intensity of FLAG-ATR normalized to GFP shows a reduction in *PIEZO1KO* cells. *N* = 4, 8 and 8 fields of view. (c) Quantification of the total area of FLAG-ATR clusters in the nucleus per cell is also reduced in *PIEZO1KO* cells. *N* = 36, 65 and 70 cells. (**d** to **f**) ATR clustering depends NOS. (d) Hypotonic stress-induced ATR clusters in WT HEK293T cells are reduced by the NOS inhibitor 1400W dihydrochloride, while histamine, a NOS activator, increases ATR clusters in *PIEZO1KO* cells. The dashed circles outline the nucleus. Scale bar = 10 μm. (e) Quantification of the fluorescence intensity of FLAG-ATR clusters. *N* = 8 fields of view. (f) Quantification of the total area of FLAG-ATR clusters in the nucleus per cell. *N* = 86, 94, 87 and 97 cells. **P* < 0.05, ***P* < 0.01, ****P* < 0.001 by two-tailed unpaired Student's t-test (b and c), One-way ANOVA followed by Tukey's multiple comparisons test (e and f).

Figure 7. Atr/mei41 functions downstream of Piezo and Nos in inhibiting axon regeneration, and NO imaging.

(**a**) Genetic interaction and epistasis analyses among *Piezo*, *Nos* and *Atr/mei41*. While class III da neuron axons in $Nos^{\Delta 15}$ heterozygotes, or transheterozygotes of *PiezoKO* and $mei41^{29D}$ ($mei41^{29D/+}$; *PiezoKO*/+) behave similarly to WT, significant enhancement of regeneration is observed in transheterozygotes of $Nos^{\Delta 15}$ and $mei41^{29D}$ ($mei41^{29D/+}$; $Nos^{\Delta 15/+}$). Class III da neuron specific overexpression of grp in *PiezoKO* or $Nos^{\Delta 15}$ mutants reduces their regeneration enhancement phenotype. On the other hand, Class III da neuron specific overexpression of mPiezo-TriM or Nos fails to suppress the regeneration enhancement in $mei41^{29D}$ mutants. The injury site is demarcated by the dashed circle. Arrow marks axon stalling while arrowheads show the regrowing axon tips. (**b**, **c**) Quantifications of class III da neuron axon regeneration with Regeneration percentage (b) and Regeneration index (c). N = 37, 8, 26, 24, 49, 31, 43, 22, 23, 22 and 27 neurons from 3 to 14 larvae. (**d** to **g**) NO imaging in WT, $Nos^{\Delta 15}$ mutants or *PiezoKO* at 48 h AI. (d) NO production is detected by DAF-FM diacetate. While in WT, NO is present around the injured axon tip, along the axon and in the cell body, the fluorescence signal is drastically reduced in $Nos^{\Delta 15}$ mutants which lacks the NO producing enzyme. (e) The NO fluorescence signal is similarly reduced in *PiezoKO*. The injury site is demarcated by the dashed circle. (f) NO fluorescence signal is rarely detected in uninjured control class III da neurons. At 48 h AI, 62.5% of the WT class III da neurons show obvious NO fluorescence signal, compared to 25% in *PiezoKO* or $Nos^{\Delta 15}$ mutants. (g) The mean NO fluorescence intensity measured at the growth cone tip is also significantly reduced in *PiezoKO* or $Nos^{\Delta 15}$ mutants. N = 8, 12 and 8 neurons from 3 to 4 larvae. *$P < 0.05$, **$P < 0.01$, ***$P < 0.001$ by Fisher's exact test (b), one-

way ANOVA followed by Holm-Sidak's test (c) or Dunnett's test (g). Scale bar = 20 μm. See also Supplementary Fig 7.

Figure 8. Inhibition of the Atr pathway by pharmacological inhibitors or conditional knockout promotes mammalian DRG neuron axon regeneration *in vitro* and *in vivo*, and axon outgrowth on substrates of differing stiffness.

(**a** to **c**) Pharmacological inhibition of Atr or Chek1 modestly enhances axon regeneration of rat embryonic DRG neurons cultured in a microfluidic chamber, when applied after injury. (a) Inhibiting Atr with AZD6738 (0.5 μM), Chek1 with VE 822 (80 nM) or MK8776 (0.2 μM) accelerates axon regeneration when imaged at 18 h AI. The axons are labeled with α-Gap43 staining. The dashed line marks the front of the axon tips in Control. (b) The axon coverage area is measured and normalized to the total width of the microgrooves. The values from the inhibitor-treated groups are further normalized to the corresponding DMSO vehicle control group in the same experiment. N = 7, 5, 5 and 5 experiments. (c) Enhanced axon regeneration is visible at 5 h AI when Atr is inhibited with AZD6738. The axons are labeled with α-Tuj1 staining. Scale bar = 100 μm. (**d**) Injection of the Chek1 inhibitor MK8776 (final concentration: ~0.3 μM) into fly larvae right after injury enhances class III da neuron axon regeneration, compared to the PBS injected control. Arrow marks retracted axon tip and arrowheads mark the regenerating axon. Scale bar = 20 μm. (**e**, **f**) Quantifications of class III da neuron axon regeneration with Regeneration percentage (e) and Regeneration index (f). N = 23 and 24 neurons from 4 larvae. (**g**, **h**) *Atr cKO* enhances sensory axon regeneration *in vivo*. Analysis of regeneration of sensory axons by SCG10 immunostaining at SNL D3. Shown are sample images of regenerating sensory axons identified by SCG10 (g) and quantification (h). SCG10

immunofluorescence intensity was measured at different distal distances and normalized to that at the lesion site as the regenerative index. Dashed line marks the lesion site. Scale bar = 100 μm. N = 6 mice for each genotype. (**i**, **j**) *Piezo1 cKO* increases adult DRG neuron axon outgrowth on hydrogels of 1 kPa, but not 30 kPa. (i) Representative images of DRG neurons (stained with the α-Tuj1 antibody) grown on substrates of different stiffness. Scale bar = 50 μm. (j) Quantification of total neurite length normalized to that of the control. N = 37, 28, 29 and 34 neurons. *P < 0.05, **P < 0.01 by Fisher's exact test (e), one-way ANOVA followed by Holm-Sidak's test (b), two-tailed unpaired Student's t-test (f and j), or Two-way ANOVA followed by Sidak's test (h).

ACKNOLODGEMENT

We thank E.J. Brown for the $Atr^{fl/fl}$ mouse; T. T. Su for fly lines; Bloomington Stock Centre, VDRC and FlyORF for fly stocks; Addgene and GenScript for plasmids; A. Patapoutian for the *PIEZO1* knockout cell line; N. Yakubovich and P. O'Farrell for the twine antibody, members of the Song lab for helpful discussions. Y. S. is a recipient of the National Institute of Neurological Disorders and Stroke (NINDS) Pathway to Independence Award. This work was supported by an IDDRC New Program Development Award (CHOP/Penn), an NINDS K99/R00 award (R00NS088211) and an NIH grant (1R01NS107392) to Y.S.

AUTHOR CONTRIBUTIONS

Conceptualization, F.L., L.M., D.L. and Y.S.; Methodology, F.L., T.Y.L., L.M., Q.W., D.L., K.P., Y.H., P.A.J and Y.S.; Investigation, F.L.,T.Y.L., L.M., Q.W., D.L., J.N., J.I.G., C.W., S.W., J.Q., S.T., M.B., P.R., G.M.T. and Y.S.; Writing – Original Draft, D.L. and Y.S.; Writing

– Review & Editing, F.L., T.Y.L., L.M., Q.W. and G.M.T.; Funding Acquisition, Y.S.; Supervision, G.M.T. and Y.S..

AUTHR INFORMATION

The authors declare no competing financial interests. Correspondence and requests for materials should be addressed to Y.S. (songy2@email.chop.edu).

The datasets generated in the current study are available from the corresponding author on reasonable request.

METHODS

Fly stocks. *19-12-Gal4*[72], *repo-Gal80* [73], *mei41*^{29D} [19], *UAS- Cdk1.T14A.Y15F*[21], *ppk-CD4-tdGFP*[74], *ppk-Gal4*[74], *Cdk1*^{B47} [22, 23], *Cdk1*$^{E1-23}$ [22, 23], *mei41::FLAG* (*PBac{fTRG01361.sfGFP-TVPTBF}VK00002*)[24], *221-Gal4*[75], *UAS-His2Av RNAi*[31], *RPA2*^{KG00759} [32], *RPA3*^{G0241} [33], *DmPiezoKO*, *UAS-Piezo RNAiv2796*[76], *nompC-QF*[77], *QUAS-mCD8GFP*[78], *QUAS-mtdTomato*[78], *ChAT-Gal4*[40], *nompC-Gal4*[77], *UAS-synaptotagmin-eGFP*[41], *Nos*$^{\Delta 15}$ [79], *UAS-mPiezo1-TriM*[17] and *UAS-Nos*[80] have been previously described. *grp*^{A196} *P{neoFRT}40A*, *UAS-grp RNAiBL27277*, *UAS-twe*, *UAS-stg*, *UAS-twe RNAiBL33044*, *UAS-twe RNAiBL36587*, *UAS-mus304 RNAiBL61355*, *tefu*$^{atm-6}$, *tefu*$^{atm-3}$, *rad50*^{EP1}, *nbs*^{1}, *mus101*^{A}, *UAS-Claspin RNAiBL32974 Hus1-like*^{MI11259} and *ctrip*^{MI14762} were from the Bloomington stock center. *UAS-mei41 RNAi*, *UAS-grp RNAiv10076*, *UAS-Rpa-70 RNAiv11210*, *UAS-Rpa-70 RNAiv110368*, *UAS-Rpa2 RNAiv102306*, *UAS-Rpa2 RNAiv30570*, *UAS-Rpa3 RNAiv101833*, *UAS-Rpa3 RNAiv15380*, *UAS-mus304 RNAiv46012*, *UAS-Rad17 RNAiv103552*, *UAS-Rad17 RNAiv44723*, *UAS-Rad1 RNAiv103430*, *UAS-Rad1 RNAiv12676*, *UAS-mus101 RNAiv31431* and *UAS-Claspin RNAiv34476* were from

691 VDRC. *UAS-RpA-70* was from FlyORF. To generate the *UAS-hATR-WT*, *UAS-hATR-KD*, *UAS-*
692 *hCHEK1*, *UAS-RPA2* and *UAS-RPA3* stocks, the entire coding sequences were cloned into the
693 pACU2 vector, and the constructs were then injected (Rainbow Transgenic Flies, Inc).
694 Randomly selected male and female larvae were used. Analyses were not performed blind to the
695 conditions of the experiments. In our study, we typically used one mutant plus one RNAi
696 knockdown, or two independent RNAi strains to confirm the phenotype of each candidate gene.
697 In addition, overexpression analysis was performed for critical genes.
698
699 **Mice.** $Atr^{fl/fl}$ [81] mice were generously provided by E.J. Brown (University of Pennsylvania).
700 *Advillin-CreER* [82] and $Piezo1^{fl/fl}$ [83] mice were obtained from Jackson Laboratories. All studies
701 and procedures involving animal subjects were performed under the approval of the Institutional
702 Animal Care and Use Committee (IACUC) at the Children's Hospital of Philadelphia. Four to
703 six week old *Avil-CreER/*$Atr^{+/+}$, *Avil-CreER/*$Atr^{fl/+}$ and *Avil-CreER/*$Atr^{fl/fl}$, or *Avil-*
704 *CreER/*$Piezo1^{+/+}$, *Avil-CreER/*$Piezo1^{fl/+}$ and *Avil-CreER/*$Piezo1^{fl/fl}$ mice were administered 2 mg
705 of tamoxifen daily by intraperitoneal injection for 5 consecutive days. SNL or DRG dissection
706 was performed approximately 2 weeks after the last tamoxifen injection. Genomic DNA from the
707 dorsal root ganglia was extracted at the end of an experiment and then analyzed by PCR to
708 confirm deletion. Age-matched mice were randomly assigned to experimental groups. Analyses
709 were not performed blind to the conditions of the experiments. All mice were housed in an
710 animal facility and maintained in a temperature controlled and light controlled environment with
711 an alternating 12 hours light/dark cycle. Up to 5 mice of the same sex from the same litter were
712 housed in a cage. The animals had no prior history of drug administration, surgery or behavioral
713 testing.

Sensory axon lesion in *Drosophila*. Da neuron axon lesion and imaging in the PNS or within the VNC were performed in live fly larvae as previously described[11, 12, 84].

Quantitative analyses of sensory axon regeneration in flies. Quantification was performed as previously described[11, 12]. Briefly, for axon regeneration in the PNS, we used "Regeneration percentage", which depicts the percent of regenerating axons among all the axons that were lesioned; "Regeneration length", which measures the increase of axon length; "Regeneration index", which is calculated as an increase of "axon length"/"distance between the cell body and the axon converging point (DCAC)" (Supplementary Fig. 1a). An axon is defined as regenerating only when it obviously regenerated beyond the retracted axon stem, and this was independently assessed of the other parameters. The regeneration parameters from various genotypes were compared to that of the WT if not noted otherwise, and only those with significant difference were labeled with the asterisks.

Live imaging in flies. Live imaging was performed as described[85, 86]. Embryos were collected for 2-24 hours on yeasted grape juice agar plates and were aged at 25°C or room temperature. At the appropriate time, a single lava was mounted in 90% glycerol under coverslips sealed with grease, imaged using a Leica SP8 or Zeiss LSM 880 microscope, and returned to grape juice agar plates between imaging sessions.

Behavioral assay. We used *NompC-Gal4/+; NompC-QF, QUAS-CD8GFP/+* larvae as control; *NompC-Gal4/UAS-Rad17 RNAiv103552; NompC-QF, QUAS-CD8GFP/UAS-Dcr2* for testing

737 *Rad17* knockdown, *mus101*^{A}*; NompC-Gal4/+; NompC-QF,QUAS-CD8GFP/+* for testing
738 *mus101* mutants, and *mei41*^{29D}*; NompC-Gal4/+; NompC-QF,QUAS-CD8GFP/+* for testing
739 *mei41* mutants. Larvae were raised at 25°C and 70% humidity. At 72 h AEL, larvae were injured
740 at the sites shown in Figure 4A. After injury, larvae were kept on grape agar plates at 25°C until
741 analysis.

742 The behavioral assay for the specific segments was modified from the method described
743 previously [38]. Briefly, an eyelash was used for delivering the gentle-touch stimulus. Based on the
744 contact area between the eyelash and larval body wall, the gentle-touch stimulus was
745 subcategorized into touch+, touch++ and touch+++ (Supplementary Fig. 6a). For each larva, the
746 injured segments (T1 and T2) were stimulated by the eyelash with touch+, touch++ and
747 touch+++, respectively (4 trials for each stimulus), followed by testing of the uninjured segments
748 (T3 and A1). The scores were recorded as "1", if stop (hesitate); "2", if recoil or turn; "3", if one
749 step back (single reverse contractile wave); "4", if two or more steps back (multiple waves of
750 reverse contraction); "0", if no response (Supplementary Fig. 6b). Only those larvae that showed
751 impaired response when stimulated at the T1 and T2 segments at 8 h AI, but retained normal
752 response at T3 and A2 segments were scored. If an injured larva scored >0 in at least two of the
753 four trials, it was defined as showing functional recovery. WT larvae showed no recovery at 24 h
754 AI and only limited recovery at 48 h AI.

755

756 **Immunohistochemistry.** Third instar larvae or cultured neurons were fixed according to
757 standard protocols. The following antibodies were used: mouse anti-p-His2Av antiserum
758 (UNC93-5.2.1, 1:100, Developmental Studies Hybridoma Bank), mouse Anti-FLAG M2 (F3165,
759 1:500, Sigma), rabbit anti-twe (1:100, O'Farrell Lab), mouse anti-Tuj1 (801202, 1:5000,

BioLegend), rabbit anti-Atrip (PA1-519, 1:400, ThermoFisher), rabbit anti-Chek1 (AV32589, 1:100, Sigma), rabbit anti-TopBP1 (LS-C663420-20, 1:1000, LSBio), α-bungarotoxin, Alexa-594 conjugate (B13423, 5 µg/mL, ThermoFisher), rabbit anti-Gap43 (NB300-143, 1:1000, Novus Biologicals), rabbit anti-SCG10 (NBP1-49461, 1:5000, Novus Biologicals), DAPI (D9542, 1:1000, Sigma) and fluorescence-conjugated secondary antibodies (1:1000, Jackson ImmunoResearch).

Quantitative RT-PCR and genotyping of *Hus1-like* insertion. Quantitative PCR (q-PCR) was done for *Hus1-like* and *rp49* according to the manufacturer's protocols. The primer sequences were as follows: *Hus1-like qPCR F* 5'-agcacttcaactccctaacg-3', *Hus1-like qPCR R* 5'-ccacatcctgtcgtacatcg-3', *rp49 qPCR F* 5'-cagtcggatcgatatgctaagctg-3' and *rp49 qPCR R* 5'-taaccgatgttgggcatcagatac-3'. The primers for *Hus1-like* genotyping were: *Genotyping primer F* 5'-gaagtggtgcacgatgttccag-3' and *Genotyping primer R* 5'-actactcccgaaaaccgcttct-3'.

Cell Culture, transfection, treatment and quantifications. WT or *PIEZO1KO* (5E3)[43] HEK293T cells were maintained in DMEM medium supplemented with 10% FBS. Cells were transfected with pcDNA3-FLAG-ATR and GFP (pLL3.7) in the presence of Lipofectamine 2000 (Invitrogen). 48 hours after transfection, cells were exposed to mock or hypotonic medium (medium diluted 1: 5 with ddH2O) for 5-7 min. In some conditions, 1400W dihydrochloride (100 µM, Santa Cruz) as a NOS inhibitor, or histamine (100 µM, Santa Cruz) as a NOS activator, were added to the hypotonic medium. For immunocytochemistry, fixed with 4% PFA for 20 min, and stained with FLAG antibody. For fluorescence intensity quantification, the integrated intensity of the whole 8-bit image was measured with ImageJ, and the FLAG-ATR fluorescence

783 intensity was normalized to that of GFP. For FLAG-ATR cluster analysis, DAPI was used to
784 define the nuclear area, and the total area of FLAG-ATR clusters per cell was measured using
785 the Analyze Particles plugin (Image J).
786
787 **NO imaging.** NO production was detected by DAF-FM diacetate (4-amino-5-methylamino-2',7'-
788 difluorofluorescein diacetate) (D23844, ThermoFisher). Fly larvae were dissected at 24 or 48 h
789 AI in PBS to expose the sensory neurons. The larval body wall – fillet prep was incubated in 10
790 μM DAF-FM diacetate for 10 min at room temperature, rinsed in PBS, fixed with 4%
791 paraformaldehyde, rinsed in PBS, and imaged by confocal microscopy. DAF-FM diacetate
792 fluorescence was quantified in ImageJ by measuring the mean gray value around the injured
793 axon tip subtracting the background fluorescence.
794
795 **Microfluidic neuron culture and axotomy.** Methods were as previously described[87]. Briefly, a
796 microfluidic culture chamber with several compartments was made using soft lithography in
797 PDMS. The axon compartment and somal compartment were separated by micrometer-sized
798 grooves. Dissociated DRG neurons from E16 rats were plated into the somal compartment. After
799 7 DIV (days *in vitro*), neurons in the somal compartment extend axons through the micro-
800 grooves and reach the axon compartment. Axotomy was performed by aspiration of the axon
801 compartment. Atr or Chek1 inhibitors were then added to the culture medium and neurons were
802 cultured for another 5 or 18 hours within the device, after which cells were fixed and stained
803 with the indicated antibodies.
804 Quantitative analysis of axon regrowth was performed as described previously[17]. In brief,
805 axons in the terminal chamber labeled by Gap43 staining were imaged using a Zeiss LSM880

laser scanning microscope with a 40× objective. Axon coverage area was calculated by connecting the tips of the distal axons. Axon coverage area was normalized to the length of the microgrooves to obtain the Normalized regeneration.

Fly larvae injection. MK8776 (S2735, selleckchem, 5 mM stock in DMSO) was dissolved in PBS before using. It was injected into larvae right after injury to a final concentration of ~0.3 μM. The final concentration of the chemical injected into larvae was calculated based on the volume estimated from larvae weight. Injection of PBS with the corresponding DMSO was the vehicle control. Injection was performed by glass micropipettes and Hamilton syringes.

Sciatic nerve lesion (SNL) and quantification of sensory axon regeneration. Mice (6 to 8 weeks old) were anesthetized and a small incision was made on the skin at the mid-thigh level. The sciatic nerve with its three major branches was exposed through a gluteal muscle splitting incision. In the sham control mouse, the posterior tibial nerve was exposed and elevated from its tissue bed, but no crush lesion was performed. In the experimental groups, the nerve crush lesion was performed on the posterior tibial nerve by freeing the nerve from connective tissue and fully crushed for 10 s. The muscle layer was closed with a 5-0 chromic gut sutures (Ethicon Inc., NJ) and the skin were closed with Autoclip® system (F.S.T. Instruments, CA).

Three days after surgery, mice were deeply anesthetized with 200 mg/kg ketamine given intraperitoneally followed by exsanguination by trans-cardiac perfusion with PBS (0.01M, pH 7.4) and fixation by paraformaldehyde (4% PFA in PBS, pH 7.4). Whole DRG (lumbar L3-L5) and full length sciatic nerve were dissected and post-fixed for 24 h and cryoprotected in sucrose solution (30% sucrose in 0.01M PBS, pH 7.4) at 4°C. Fixed DRG and sciatic nerve tissues were

829 embedded in Optimal Cutting Temperature O.C.T Compound (Leica, Germany) and sectioned at
830 14 µm using Leica CM3050 (Leica, Germany). DRGs was later processed as floating sections
831 and sagittal sciatic nerve sections were thaw-mounted on gelatin-dodecahydrate treated glass
832 microscope slides (Superfrost Plus, Fisher Scientific).

833 To measure regeneration of the sciatic nerve, sections were stained with the α-SCG10
834 antibody. SCG10 intensity was measured by ImageJ and the average intensities were calculated
835 across 100 µm non-overlapping regions and normalized. The regenerative index was calculated
836 as previously described[88].

837

838 **Stiffness assay.** Polyacrylamide (PAA) hydrogels were made as described by[57, 89] with some
839 modifications. Briefly, 18 mm circular glass coverslips (NeuVitro, Vancouver, WA) were treated
840 with 3-aminopropyl-trimethoxysilane (Fisher Scientific), extensively washed with Milli-Q H_20,
841 and treated with 0.5% glutaraldehyde (Fisher Scientific). Rectangular 22 x 50 mm glass
842 coverslips (Fisher Scientific) were treated with hydrocarbon soluble siliconizing solution to
843 make non-adhesive top coverslips. Next, 40% Acrylamide and 2% bis-acrylamide (Bio-Rad
844 Laboratories, Richmond, CA) were mixed at ratios of 5%, 0.1% and 12%, 0.4% to achieve gels
845 of 1.0 and 30.0 kPa stiffnesses, respectively[89]. Polymerization was initiated by adding
846 ammonium persulfate (APS, stock concentration of 10% w/v, ThermoFisher) and N,N,N,N-
847 tetramethylelthylenediamine (TEMED, AcrosOrganics, Morris Plains, NJ). After initiation, 80
848 µL of gel solution was transferred to each siliconized (bottom) coverslip and covered with the
849 nonadhesive top coverslip. After 15 minutes, the bottom coverslips were removed, revealing
850 hydrogels attached to only the top coverslip. Gels were allowed to swell in Milli-Q H2O for 1 h
851 at 37˚C and coated in sulfosuccinimidyl6-(40 -azido-20 -nitrophenylamino) hexanoate (sulfo-

SANPAH, ThermoFisher) and photoactivated with 365 nm UV light for 10 minutes. PAA gels were gently washed with Milli-Q H_2O and coated in 0.1 mg/mL Poly-L-Lysine overnight in a 37˚C, 5% CO_2, and humidity-controlled incubator. On the day of cell seeding, the PAA gels were coated in 5 µg/mm^2 laminin (20 µL of 1 mg/mL laminin in 1000 mL growth medium) for 6 hours, 37˚C.

DRG primary culture was performed according to[56]. Briefly, anesthetized mice were perfused with chilled, sterile PBS, and DRGs were dissected and washed in cold HBSS. DRG tissues were digested and incubated for 21 minutes at 37˚C in a solution containing 1 mg L-cysteine (Sigma-Aldrich), 60U Papain (Worthington Biochemical Corporation), 1 µg DNase I (Fisher Scientific) in 1.5 mL Ca^{2+}/Mg^{2+}-free HBSS. The DRG tissues were pelleted (250x g, 3 minutes, room temperature) and resuspended and further digested (37˚C, 20 minutes) in an enzyme cocktail containing 15 mg dispase II (Sigma-Aldrich) and 12 mg of collagenase (Worthington Biochemical Corporation) in 3 mL of Ca^{2+}/Mg^{2+}-free HBSS. The dispase/collagenase solution was inactivated by the addition of a 1:1 ratio of tissue solution to prewarmed Neurobasal A medium (1x Glutamax, B27 supplement, 10% FBS). The cell solution was passed through a 70 µm cell strainer (ThermoFisher), pelleted (250x g, 3 minutes, room temperature), and resuspended in culture medium (Neurobasal A, B27, Glutamax, 10% FBS, 100 ng/mL neural growth factor; mouse NGF 7.0s, Millipore Sigma). DRG neurons were then seeded on each corresponding PAA hydrogel at approximately 30,000 cells per 250 mm^2 growth area to achieve single cell density. Primary DRG neurons were cultured on PAA gels for 38-40 hours before fixed in pre-warmed 4% sucrose/4% PFA in 1x PBS for 10 minutes at room temperature. Cells were permeabilized in 0.2% Triton X-100 in TBS (10 minutes, room temperature) and

blocked in 10% normal donkey serum in PBS (2 h, room temperature) and stained with α-Tuj1 antibody.

Neurons were imaged on a Zeiss LSM 880 confocal laser scanning microscope and image acquisition occurred within 48 hours of mounting each hydrogel. Each image's maximum projection image was used during analysis of neurite lengths. The total neurite length was measured with ImageJ's plugin program, "Simple Neurite Tracer"[90], and normalized to the mean of the control.

Quantification and statistical analysis. No statistical methods were used to pre-determine sample sizes but our sample sizes are similar to those reported in previous publications[11, 12], and the statistical analyses were done afterwards without interim data analysis. Data distribution was assumed to be normal but this was not formally tested. All data were collected and processed randomly. Each experiment was successfully reproduced at least three times and was performed on different days. The values of ''N'' (sample size) are provided in the figure legends. Data are expressed as mean ± SEM in bar graphs. No data points were excluded. Two-tailed unpaired Student's t-test was performed for comparison between two groups of samples. One-way ANOVA followed by multiple comparison test was performed for comparisons among three or more groups of samples. Two-way ANOVA followed by multiple comparison test was performed for comparisons between two or more curves. Fisher's exact test was used to compare the percentage. Statistical significance was assigned, $*P < 0.05$, $**P < 0.01$, $***P < 0.001$.

SUPPLEMENTARY INFORMATION

Supplementary Figures 1-8

Supplementary Videos 1-6

SUPPLEMENTARY FIGURE LEGENDS

Supplementary Figure 1. Related to Figure 1. Quantification of sensory axon regeneration in the fly PNS, dendrite branching and mei41 expression.

(**a**) "Regeneration index" is calculated as an increase of "axon length"/"distance between the cell body and the axon converging point (DCAC)". (b) The dendrite of class III da neuron of various genotypes were traced at 72 h AI and the total dendrite length was quantified. *N* = 20, 15, 15 and 10 neurons from 3 to 5 larvae. (**c**) Expression and localization of mei41 with and without injury. Mei41 is present mainly in the nucleus of class III da sensory neurons. No significant difference is observed after axon injury. The injury site is demarcated by the green dashed circle. Class III and IV da neurons are outlined by the red and yellow dashed lines, respectively. *N* = 8 segments from 4 larvae. No statistical difference is detected by One-way ANOVA followed by Dunnett's test (b).

Supplementary Figure 2. Related to Figure 2. The Atm/tefu pathway does not regulate axon regeneration in da sensory neurons in flies, and class I da neuron axon regeneration.

(**a**, **b**) Inhibiting the Atm/tefu pathway does not significantly alter class IV da neuron axon regeneration. Quantifications of class IV da neuron axon regeneration with Regeneration percentage (a) and Regeneration index (b). *N* = 27, 17, 19 and 18 neurons from 5 to 7 larvae. (**c** to **e**) Atm/tefu loss of function does not promote class III da neuron axon regeneration. (c) Atm/tefu removal as in $tefu^{atm\text{-}6/atm\text{-}3}$ mutants does not increase axon regeneration. The injury site is demarcated by the dashed circle. Arrow marks axon stalling. Scale bar = 20 μm.

Quantifications of class III da neuron axon regeneration with Regeneration percentage (d) and Regeneration index (e), shown in the scatter plot. $N = 23$ and 22 neurons from 7 to 8 larvae. No statistical difference is detected by Fisher's exact test (a and d), one-way ANOVA followed by Dunnett's test (b), two-tailed unpaired Student's t-test (e). (**f** to **h**) *PiezoKO* and *mei41*^{29D} mutants enhance class I da neuron axon regeneration. The injury site is demarcated by the dashed circle. Arrowheads mark regenerating axons. Scale bar = 20 μm. Quantifications of class I da neuron axon regeneration with Regeneration percentage (g) and Regeneration index (h). $N = 40$, 31 and 26 neurons from 7 to 11 larvae. *$P < 0.05$, **$P < 0.01$ by Fisher's exact test (g), one-way ANOVA followed by Dunnett's test (h).

Supplementary Figure 3. Related to Figure 2. Overexpression of RPAs does not reduce axon regeneration.

Quantifications of class IV da neuron axon regeneration with Regeneration percentage (a) and Regeneration index (b). $N = 31$, 29, 26 and 24 neurons from 7 to 8 larvae. No statistical difference is detected by Fisher's exact test (a), one-way ANOVA followed by Dunnett's test (b).

Supplementary Figure 4. Related to Figure 3. The insertional allele of Hus1-like – *Hus1-like*^{MI11259} is a loss of function mutant, and *ctrip* mutants do not show increased axon regeneration.

(**a**) The *Hus1-like*^{MI11259} insertional locus, and primers for genotyping and quantitative RT-PCR. (**b**) Genomic PCR using the genotyping primers confirms the insertion. (**c**) Quantitative RT-PCR shows significant reduction of the *Hus1-like* transcripts in the *Hus1-like*^{MI11259} mutants. *rp49* was used as the loading control, and the *Hus1-like* mRNA level was normalized to that of WT. $N = 3$

943 biological replicates from 5-10 larvae each. .*$P < 0.05$, by two-tailed unpaired Student's t-test.
944 (**d**) Quantifications of class III da neuron axon regeneration with Regeneration percentage and
945 Regeneration index. $N = 23$ and 27 neurons from 6 to 7 larvae. No statistical difference is
946 detected by Fisher's exact test or two-tailed unpaired Student's t-test.
947
948 **Supplementary Figure 5. Related to Figure 3. The expression pattern of Atr pathway**
949 **members in fly, mouse and human.**
950 (**a**) Expression and localization of twe with or without injury. Twe is present mainly in the
951 nucleus of class III da sensory neurons. No significant difference is observed after axon injury.
952 The injury site is demarcated by the green dashed circle. Class III da neuron cell bodies are
953 outlined by the red dashed circle. Twe is also expressed in other da neurons. Scale bar = 20 μm.
954 (**b**) Immunostaining for Atrip, Chek1 and TopBP1 using mouse DRG tissue sections. All three
955 are expressed with or without sciatic nerve lesion (SNL). DRG neurons were counterstained with
956 the α-Tuj1 antibody. Scale bar = 20 μm. (**c**) Expression level of Atr pathway members in
957 various tissues in mouse and human. All of them are expressed in the mouse and human DRG,
958 although at a low to median level.
959
960 **Supplementary Figure 6. Related to Figures 4 and 5. The modified gentle-touch behavioral**
961 **paradigm for assessing functional recovery after CNS injury in flies.**
962 (**a**) The definition of the gentle-touch stimulus. The intensity of the stimulation is subcategorized
963 based on the contact area between the eyelash and the body segment: touch+, touch++ and
964 touch+++, with the eyelash diameter covering <1/8, 1/8-1/4 or 1/4-1/2 of the segment,
965 respectively. (**b**) The scoring system for the gentle-touch response – gently touching larval

anterior segments with an eyelash elicits a set of stereotypical response. While the larvae are moving forward, by gentle touch, if they stop (hesitate), score 1; recoil or turn, score 2; one step back (single reverse contractile wave), score 3; two or more steps back (multiple waves of reverse contraction), score 4; no response, score 0. (**c**) Injuring the class III da neuron axon bundle at T1 or T2 in the VNC leads to impaired touch response specifically at segment T1 or T2, without affecting neighboring segments. Total response scores from 4 trials are added and shown in scatter plots. N = 10 larvae. (**d** to **f**) The behavioral response in the uninjured T3 and A1 segments are comparable among the different genotypes – $mus101^{A}$ mutants (d), class III da neuron specific *Rad17* RNAi (e) and $mei41^{29D}$ mutants (f). Larvae also show a graded response according to the stimulation intensity. N = 41 larvae for Ctrl, 23 for $mus101^{A}$, 33 for $mei41^{29D}$, 11, 26 and 26 for *Rad17 RNAi* at 8 h, 24 h and 48 h. *$P < 0.05$, **$P < 0.01$, ***$P < 0.001$ by one-way ANOVA followed by Tukey's test (c to f). (**g**) Class III da neurons are co-labeled by *nompC-QF>mCD8GFP* (the class III da neuron marker) and *ChAT-Gal4>CD4TdTomato*. Arrowhead marks the class III da neuron cell body. Scale bar = 20 μm.

Supplementary Figure 7. Related to Figure 7. NO imaging in uninjured class III da neurons does not show significant difference among WT, *PiezoKO* and $Nos^{\Delta 15}$ mutants. No obvious NO fluorescence signal is detected in uninjured class III da neurons. N = 8, 12 and 8 neurons from 3 to 4 larvae. Scale bar = 20 μm.

Supplementary Figure 8. The proposed Piezo-Nos-Atr-Chek1 pathway in inhibiting axon regeneration. The proposed Piezo-Nos-Atr-Chek1 signaling cascade that inhibits axon regeneration. During axon regeneration, the mechanical force resulting from the interactions

between the growth cone and the environment, activates the mechanosensitive ion channel Piezo at the growth cone tip, leading to local calcium influx and activation of Nos, which then produces NO. NO functions as a second messenger and propagates to the nucleus where it activates Atr and the associated checkpoint complex. Atr then phosphorylates and activates Chek1, which phosphorylates and inactivates Cdc25, inhibiting its ability to dephosphorylate and activate Cdk1. The phosphorylated and inactive Cdk1 suppresses axon regeneration through downstream effectors.

Supplementary Videos 1-6. The gentle-touch behavioral assay for assessing functional recovery after CNS injury.

Supplementary Video 1. Related to Figure 4 and Supplementary Figure 6. WT 8 h AI

Supplementary Video 2. Related to Figure 4 and Supplementary Figure 6. WT 48 h AI

Supplementary Video 3. Related to Figures 4 and Supplementary Figure 6. *Mus101*^{A} mutants 8 h AI

Supplementary Video 4. Related to Figures 4 and Supplementary Figure 6. *Mus101*^{A} mutants 48 h AI

Supplementary Video 5. Related to Figures 4 and Supplementary Figure 6. Class III da neuron specific *Rad17* RNAi 8 h AI

Supplementary Video 6. Related to Figures 4 and Supplementary Figure 6. Class III da neuron specific *Rad17* RNAi 48 h AI

REFERENCES

1. Liu, K., Tedeschi, A., Park, K.K. & He, Z. Neuronal intrinsic mechanisms of axon regeneration. *Annu Rev Neurosci* **34**, 131-152 (2011).

2. Di Giovanni, S. Molecular targets for axon regeneration: focus on the intrinsic pathways. *Expert Opin Ther Targets* **13**, 1387-1398 (2009).
3. Schwab, M.E. & Strittmatter, S.M. Nogo limits neural plasticity and recovery from injury. *Curr Opin Neurobiol* **27**, 53-60 (2014).
4. Tedeschi, A. & Bradke, F. Spatial and temporal arrangement of neuronal intrinsic and extrinsic mechanisms controlling axon regeneration. *Curr Opin Neurobiol* **42**, 118-127 (2017).
5. Mahar, M. & Cavalli, V. Intrinsic mechanisms of neuronal axon regeneration. *Nat Rev Neurosci* **19**, 323-337 (2018).
6. Terzis, J.K. & Kokkalis, Z.T. Selective contralateral c7 transfer in posttraumatic brachial plexus injuries: a report of 56 cases. *Plast Reconstr Surg* **123**, 927-938 (2009).
7. Songcharoen, P., Wongtrakul, S., Mahaisavariya, B. & Spinner, R.J. Hemi-contralateral C7 transfer to median nerve in the treatment of root avulsion brachial plexus injury. *J Hand Surg Am* **26**, 1058-1064 (2001).
8. Lundborg, G. A 25-year perspective of peripheral nerve surgery: evolving neuroscientific concepts and clinical significance. *J Hand Surg Am* **25**, 391-414 (2000).
9. Painter, M.W. *et al.* Diminished Schwann cell repair responses underlie age-associated impaired axonal regeneration. *Neuron* **83**, 331-343 (2014).
10. He, Z. & Jin, Y. Intrinsic Control of Axon Regeneration. *Neuron* **90**, 437-451 (2016).
11. Song, Y. *et al.* Regeneration of Drosophila sensory neuron axons and dendrites is regulated by the Akt pathway involving Pten and microRNA bantam. *Genes Dev* **26**, 1612-1625 (2012).
12. Song, Y. *et al.* Regulation of axon regeneration by the RNA repair and splicing pathway. *Nat Neurosci* **18**, 817-825 (2015).
13. Fulda, S., Gorman, A.M., Hori, O. & Samali, A. Cellular stress responses: cell survival and cell death. *Int J Cell Biol* **2010**, 214074 (2010).
14. Donzelli, M. & Draetta, G.F. Regulating mammalian checkpoints through Cdc25 inactivation. *EMBO Rep* **4**, 671-677 (2003).
15. Zou, L. Single- and double-stranded DNA: building a trigger of ATR-mediated DNA damage response. *Genes Dev* **21**, 879-885 (2007).
16. Kumar, A. *et al.* ATR mediates a checkpoint at the nuclear envelope in response to mechanical stress. *Cell* **158**, 633-646 (2014).
17. Song, Y. *et al.* The Mechanosensitive Ion Channel Piezo Inhibits Axon Regeneration. *Neuron* (2019).
18. Syeda, R. *et al.* Piezo1 Channels Are Inherently Mechanosensitive. *Cell Rep* **17**, 1739-1746 (2016).
19. Laurencon, A., Purdy, A., Sekelsky, J., Hawley, R.S. & Su, T.T. Phenotypic analysis of separation-of-function alleles of MEI-41, Drosophila ATM/ATR. *Genetics* **164**, 589-601 (2003).
20. Lee, T. & Luo, L. Mosaic analysis with a repressible cell marker for studies of gene function in neuronal morphogenesis. *Neuron* **22**, 451-461 (1999).
21. Ayeni, J.O. *et al.* Dual phosphorylation of cdk1 coordinates cell proliferation with key developmental processes in Drosophila. *Genetics* **196**, 197-210 (2014).
22. Clegg, N.J., Whitehead, I.P., Williams, J.A., Spiegelman, G.B. & Grigliatti, T.A. A developmental and molecular analysis of Cdc2 mutations in Drosophila melanogaster. *Genome* **36**, 676-685 (1993).

23. Stern, B., Ried, G., Clegg, N.J., Grigliatti, T.A. & Lehner, C.F. Genetic analysis of the Drosophila cdc2 homolog. *Development* **117**, 219-232 (1993).
24. Sarov, M. *et al.* A genome-wide resource for the analysis of protein localisation in Drosophila. *Elife* **5**, e12068 (2016).
25. Silva, E. *et al.* ATM is required for telomere maintenance and chromosome stability during Drosophila development. *Curr Biol* **14**, 1341-1347 (2004).
26. Ciapponi, L. *et al.* The Drosophila Mre11/Rad50 complex is required to prevent both telomeric fusion and chromosome breakage. *Curr Biol* **14**, 1360-1366 (2004).
27. Bi, X. *et al.* Drosophila ATM and ATR checkpoint kinases control partially redundant pathways for telomere maintenance. *Proc Natl Acad Sci U S A* **102**, 15167-15172 (2005).
28. Bonner, W.M. *et al.* GammaH2AX and cancer. *Nat Rev Cancer* **8**, 957-967 (2008).
29. Kuo, L.J. & Yang, L.X. Gamma-H2AX - a novel biomarker for DNA double-strand breaks. *In Vivo* **22**, 305-309 (2008).
30. Lake, C.M., Holsclaw, J.K., Bellendir, S.P., Sekelsky, J. & Hawley, R.S. The development of a monoclonal antibody recognizing the Drosophila melanogaster phosphorylated histone H2A variant (gamma-H2AV). *G3 (Bethesda)* **3**, 1539-1543 (2013).
31. Neely, G.G. *et al.* A genome-wide Drosophila screen for heat nociception identifies alpha2delta3 as an evolutionarily conserved pain gene. *Cell* **143**, 628-638 (2010).
32. Crest, J., Oxnard, N., Ji, J.Y. & Schubiger, G. Onset of the DNA replication checkpoint in the early Drosophila embryo. *Genetics* **175**, 567-584 (2007).
33. Zhou, L. & Luo, H. Replication protein a links cell cycle progression and the onset of neurogenesis in Drosophila optic lobe development. *J Neurosci* **33**, 2873-2888 (2013).
34. Farrell, J.A. & O'Farrell, P.H. Mechanism and regulation of Cdc25/Twine protein destruction in embryonic cell-cycle remodeling. *Curr Biol* **23**, 118-126 (2013).
35. Flegel, C. *et al.* RNA-Seq Analysis of Human Trigeminal and Dorsal Root Ganglia with a Focus on Chemoreceptors. *PLoS One* **10**, e0128951 (2015).
36. Ray, P. *et al.* Comparative transcriptome profiling of the human and mouse dorsal root ganglia: an RNA-seq-based resource for pain and sensory neuroscience research. *Pain* **159**, 1325-1345 (2018).
37. Hao, Y. & Collins, C. Intrinsic mechanisms for axon regeneration: insights from injured axons in Drosophila. *Curr Opin Genet Dev* **44**, 84-91 (2017).
38. Kernan, M., Cowan, D. & Zuker, C. Genetic dissection of mechanosensory transduction: mechanoreception-defective mutations of Drosophila. *Neuron* **12**, 1195-1206 (1994).
39. Yan, Z. *et al.* Drosophila NOMPC is a mechanotransduction channel subunit for gentle-touch sensation. *Nature* **493**, 221-225 (2013).
40. Salvaterra, P.M. & Kitamoto, T. Drosophila cholinergic neurons and processes visualized with Gal4/UAS-GFP. *Brain Res Gene Expr Patterns* **1**, 73-82 (2001).
41. Zhang, Y.Q., Rodesch, C.K. & Broadie, K. Living synaptic vesicle marker: synaptotagmin-GFP. *Genesis* **34**, 142-145 (2002).
42. Couton, L. *et al.* Development of connectivity in a motoneuronal network in Drosophila larvae. *Curr Biol* **25**, 568-576 (2015).
43. Dubin, A.E. *et al.* Endogenous Piezo1 Can Confound Mechanically Activated Channel Identification and Characterization. *Neuron* **94**, 266-270 e263 (2017).
44. Garvey, E.P. *et al.* 1400W is a slow, tight binding, and highly selective inhibitor of inducible nitric-oxide synthase in vitro and in vivo. *J Biol Chem* **272**, 4959-4963 (1997).

45. Lantoine, F., Iouzalen, L., Devynck, M.A., Millanvoye-Van Brussel, E. & David-Dufilho, M. Nitric oxide production in human endothelial cells stimulated by histamine requires Ca2+ influx. *Biochem J* **330 (Pt 2)**, 695-699 (1998).
46. Wang, X., Zalcenstein, A. & Oren, M. Nitric oxide promotes p53 nuclear retention and sensitizes neuroblastoma cells to apoptosis by ionizing radiation. *Cell Death Differ* **10**, 468-476 (2003).
47. Jaszczak, J.S., Wolpe, J.B., Dao, A.Q. & Halme, A. Nitric Oxide Synthase Regulates Growth Coordination During Drosophila melanogaster Imaginal Disc Regeneration. *Genetics* **200**, 1219-1228 (2015).
48. Jaszczak, J.S., Wolpe, J.B., Bhandari, R., Jaszczak, R.G. & Halme, A. Growth Coordination During Drosophila melanogaster Imaginal Disc Regeneration Is Mediated by Signaling Through the Relaxin Receptor Lgr3 in the Prothoracic Gland. *Genetics* **204**, 703-709 (2016).
49. Zhou, B. *et al.* Facilitation of axon regeneration by enhancing mitochondrial transport and rescuing energy deficits. *J Cell Biol* **214**, 103-119 (2016).
50. Holland, S.M. *et al.* Palmitoylation controls DLK localization, interactions and activity to ensure effective axonal injury signaling. *Proc Natl Acad Sci U S A* **113**, 763-768 (2016).
51. Weber, A.M. & Ryan, A.J. ATM and ATR as therapeutic targets in cancer. *Pharmacol Ther* **149**, 124-138 (2015).
52. Manic, G., Obrist, F., Sistigu, A. & Vitale, I. Trial Watch: Targeting ATM-CHK2 and ATR-CHK1 pathways for anticancer therapy. *Mol Cell Oncol* **2**, e1012976 (2015).
53. Daud, A.I. *et al.* Phase I dose-escalation trial of checkpoint kinase 1 inhibitor MK-8776 as monotherapy and in combination with gemcitabine in patients with advanced solid tumors. *J Clin Oncol* **33**, 1060-1066 (2015).
54. Weiss, G.J. *et al.* Phase I dose-escalation study to examine the safety and tolerability of LY2603618, a checkpoint 1 kinase inhibitor, administered 1 day after pemetrexed 500 mg/m(2) every 21 days in patients with cancer. *Invest New Drugs* **31**, 136-144 (2013).
55. Shin, J.E., Geisler, S. & DiAntonio, A. Dynamic regulation of SCG10 in regenerating axons after injury. *Exp Neurol* **252**, 1-11 (2014).
56. Malin, S.A., Davis, B.M. & Molliver, D.C. Production of dissociated sensory neuron cultures and considerations for their use in studying neuronal function and plasticity. *Nat Protoc* **2**, 152-160 (2007).
57. Kandow, C.E., Georges, P.C., Janmey, P.A. & Beningo, K.A. Polyacrylamide hydrogels for cell mechanics: steps toward optimization and alternative uses. *Methods Cell Biol* **83**, 29-46 (2007).
58. Koch, D., Rosoff, W.J., Jiang, J., Geller, H.M. & Urbach, J.S. Strength in the periphery: growth cone biomechanics and substrate rigidity response in peripheral and central nervous system neurons. *Biophys J* **102**, 452-460 (2012).
59. Polackwich, R.J., Koch, D., McAllister, R., Geller, H.M. & Urbach, J.S. Traction force and tension fluctuations in growing axons. *Front Cell Neurosci* **9**, 417 (2015).
60. Moeendarbary, E. *et al.* The soft mechanical signature of glial scars in the central nervous system. *Nat Commun* **8**, 14787 (2017).
61. Yuan, Z. *et al.* Activation of FOXO1 by Cdk1 in cycling cells and postmitotic neurons. *Science* **319**, 1665-1668 (2008).
62. Byrne, A.B. *et al.* Insulin/IGF1 signaling inhibits age-dependent axon regeneration. *Neuron* **81**, 561-573 (2014).

63. Wynne, C.L. & Vallee, R.B. Cdk1 phosphorylation of the dynein adapter Nde1 controls cargo binding from G2 to anaphase. *J Cell Biol* **217**, 3019-3029 (2018).
64. Ducommun Priest, M., Navarro, M.F., Bremer, J. & Granato, M. Dynein promotes sustained axonal growth and Schwann cell remodeling early during peripheral nerve regeneration. *PLoS Genet* **15**, e1007982 (2019).
65. Blanquie, O. & Bradke, F. Cytoskeleton dynamics in axon regeneration. *Curr Opin Neurobiol* **51**, 60-69 (2018).
66. Di Giovanni, S. *et al.* The tumor suppressor protein p53 is required for neurite outgrowth and axon regeneration. *EMBO J* **25**, 4084-4096 (2006).
67. Byrne, A.B. *et al.* Inhibiting poly(ADP-ribosylation) improves axon regeneration. *Elife* **5** (2016).
68. Wang, X. *et al.* Inhibition of Poly-ADP-Ribosylation Fails to Increase Axonal Regeneration or Improve Functional Recovery after Adult Mammalian CNS Injury. *eNeuro* **3** (2016).
69. Martin, L.J., Chen, K. & Liu, Z. Adult motor neuron apoptosis is mediated by nitric oxide and Fas death receptor linked by DNA damage and p53 activation. *J Neurosci* **25**, 6449-6459 (2005).
70. Kidiyoor, G.R., Kumar, A. & Foiani, M. ATR-mediated regulation of nuclear and cellular plasticity. *DNA repair* **44**, 143-150 (2016).
71. Shanske, A., Caride, D.G., Menasse-Palmer, L., Bogdanow, A. & Marion, R.W. Central nervous system anomalies in Seckel syndrome: report of a new family and review of the literature. *American journal of medical genetics* **70**, 155-158 (1997).
72. Xiang, Y. *et al.* Light-avoidance-mediating photoreceptors tile the Drosophila larval body wall. *Nature* **468**, 921-926 (2010).
73. Awasaki, T., Lai, S.L., Ito, K. & Lee, T. Organization and postembryonic development of glial cells in the adult central brain of Drosophila. *J Neurosci* **28**, 13742-13753 (2008).
74. Han, C., Jan, L.Y. & Jan, Y.N. Enhancer-driven membrane markers for analysis of nonautonomous mechanisms reveal neuron-glia interactions in Drosophila. *Proc Natl Acad Sci U S A* **108**, 9673-9678 (2011).
75. Grueber, W.B., Jan, L.Y. & Jan, Y.N. Different levels of the homeodomain protein cut regulate distinct dendrite branching patterns of Drosophila multidendritic neurons. *Cell* **112**, 805-818 (2003).
76. Kim, S.E., Coste, B., Chadha, A., Cook, B. & Patapoutian, A. The role of Drosophila Piezo in mechanical nociception. *Nature* **483**, 209-212 (2012).
77. Petersen, L.K. & Stowers, R.S. A Gateway MultiSite recombination cloning toolkit. *PLoS One* **6**, e24531 (2011).
78. Potter, C.J., Tasic, B., Russler, E.V., Liang, L. & Luo, L. The Q system: a repressible binary system for transgene expression, lineage tracing, and mosaic analysis. *Cell* **141**, 536-548 (2010).
79. Yakubovich, N., Silva, E.A. & O'Farrell, P.H. Nitric oxide synthase is not essential for Drosophila development. *Curr Biol* **20**, R141-142 (2010).
80. Lacin, H. *et al.* Genome-wide identification of Drosophila Hb9 targets reveals a pivotal role in directing the transcriptome within eight neuronal lineages, including activation of nitric oxide synthase and Fd59a/Fox-D. *Dev Biol* **388**, 117-133 (2014).
81. Ruzankina, Y. *et al.* Deletion of the developmentally essential gene ATR in adult mice leads to age-related phenotypes and stem cell loss. *Cell Stem Cell* **1**, 113-126 (2007).

82. Lau, J. *et al.* Temporal control of gene deletion in sensory ganglia using a tamoxifen-inducible Advillin-Cre-ERT2 recombinase mouse. *Mol Pain* **7**, 100 (2011).
83. Cahalan, S.M. *et al.* Piezo1 links mechanical forces to red blood cell volume. *Elife* **4** (2015).
84. Stone, M.C., Albertson, R.M., Chen, L. & Rolls, M.M. Dendrite injury triggers DLK-independent regeneration. *Cell reports* **6**, 247-253 (2014).
85. Emoto, K., Parrish, J.Z., Jan, L.Y. & Jan, Y.N. The tumour suppressor Hippo acts with the NDR kinases in dendritic tiling and maintenance. *Nature* **443**, 210-213 (2006).
86. Parrish, J.Z., Emoto, K., Kim, M.D. & Jan, Y.N. Mechanisms that regulate establishment, maintenance, and remodeling of dendritic fields. *Annu Rev Neurosci* **30**, 399-423 (2007).
87. Park, J.W., Vahidi, B., Taylor, A.M., Rhee, S.W. & Jeon, N.L. Microfluidic culture platform for neuroscience research. *Nature protocols* **1**, 2128-2136 (2006).
88. Weng, Y.L. *et al.* An Intrinsic Epigenetic Barrier for Functional Axon Regeneration. *Neuron* **94**, 337-346 e336 (2017).
89. Pogoda, K. *et al.* Soft Substrates Containing Hyaluronan Mimic the Effects of Increased Stiffness on Morphology, Motility, and Proliferation of Glioma Cells. *Biomacromolecules* **18**, 3040-3051 (2017).
90. Longair, M.H., Baker, D.A. & Armstrong, J.D. Simple Neurite Tracer: open source software for reconstruction, visualization and analysis of neuronal processes. *Bioinformatics* **27**, 2453-2454 (2011).

Figure 1

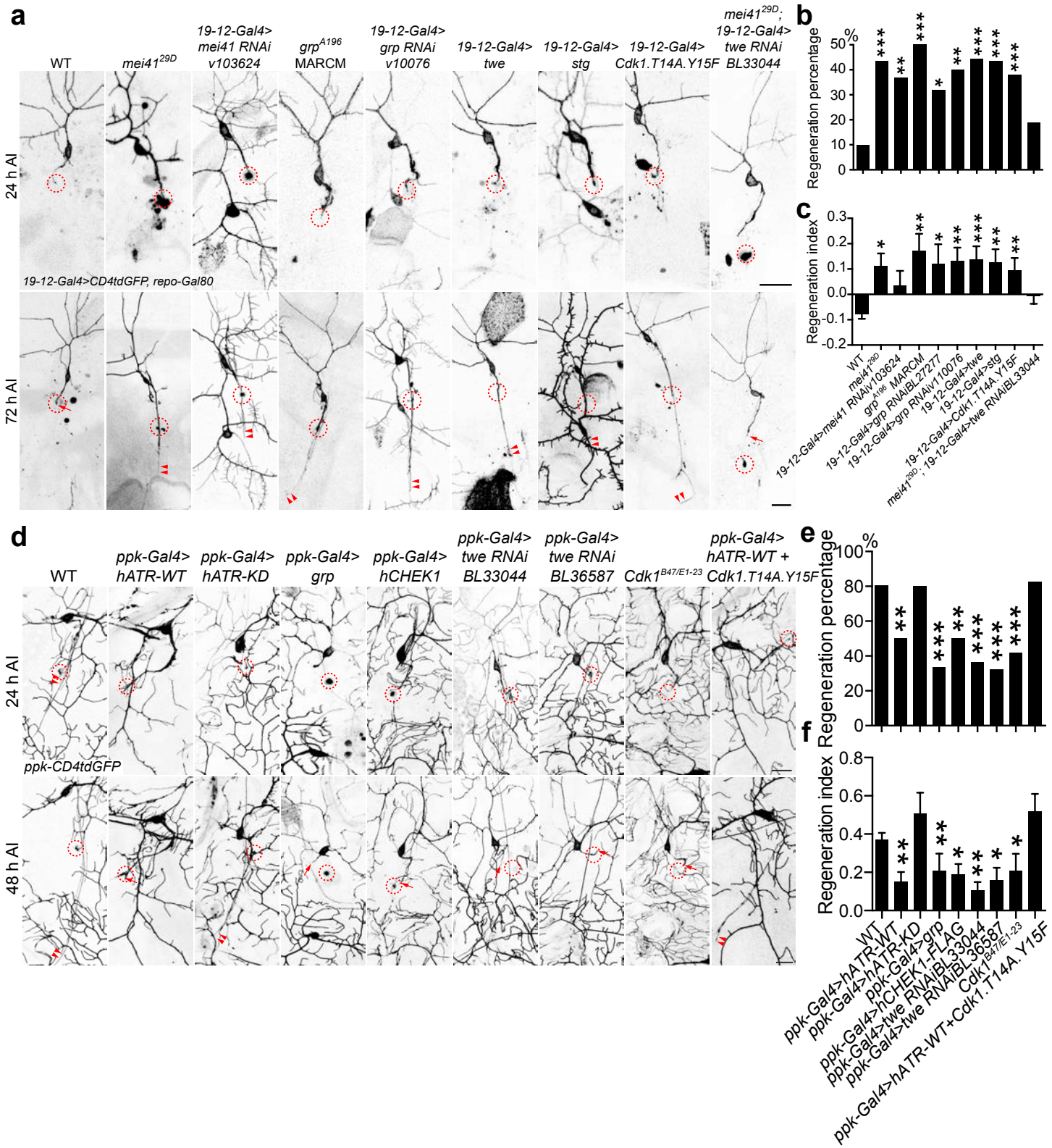

Figure 2

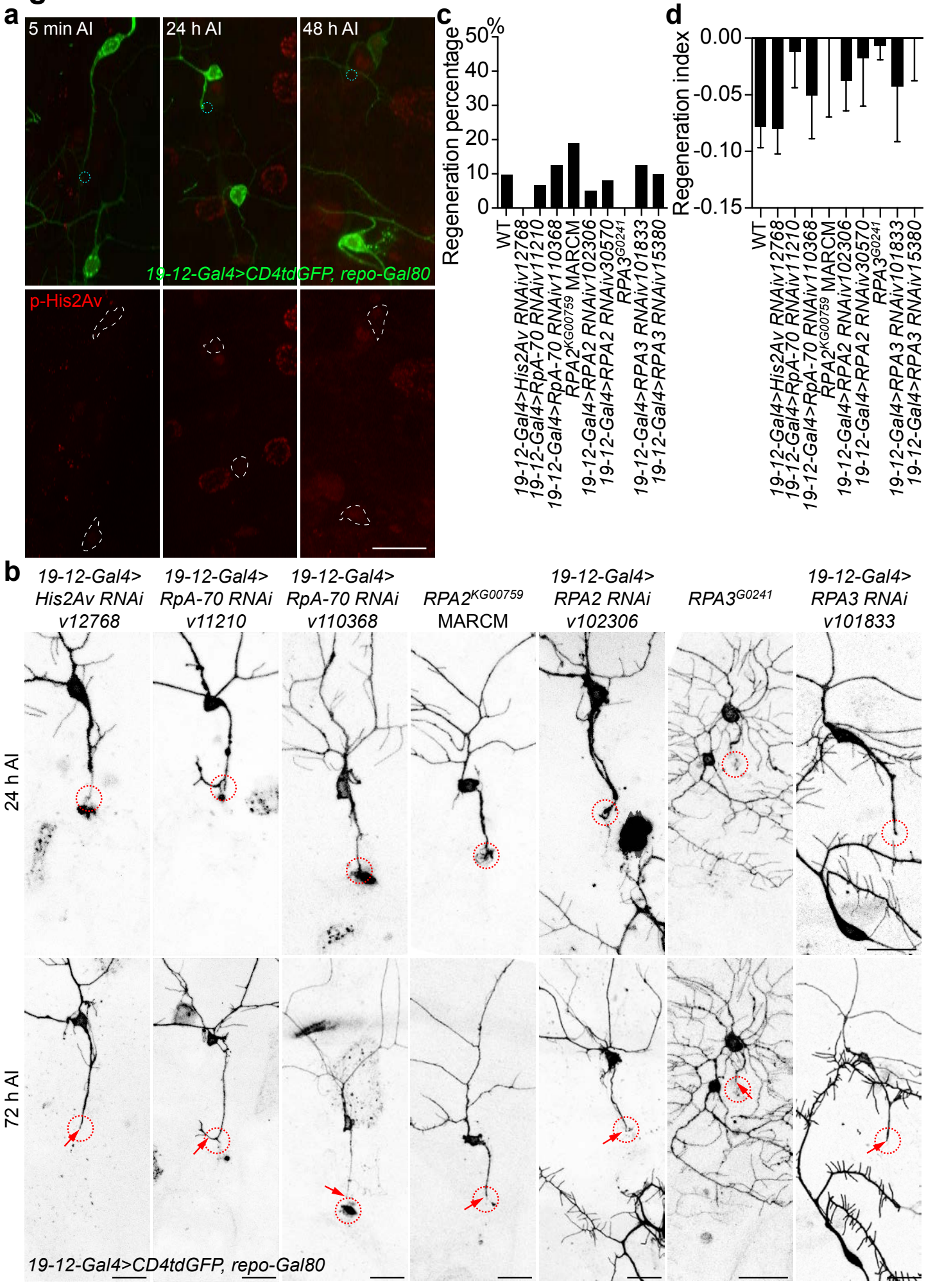

Figure 3

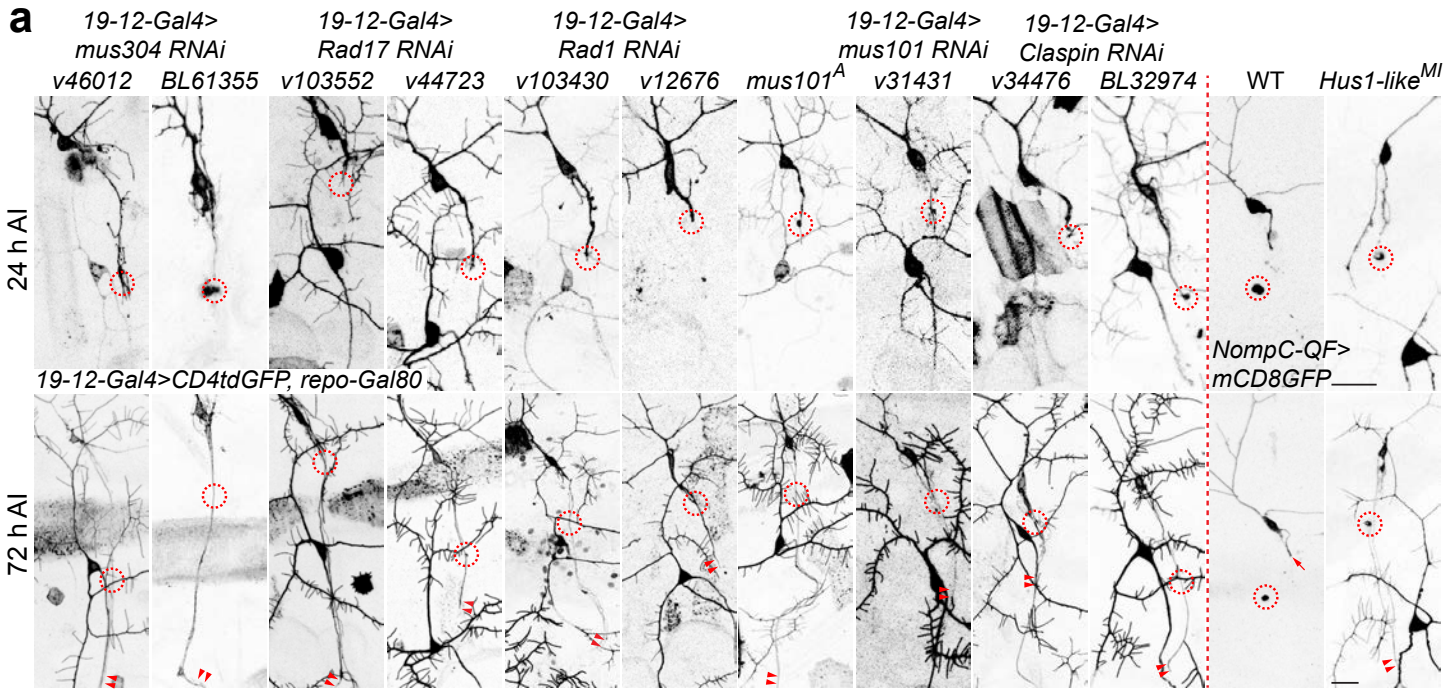

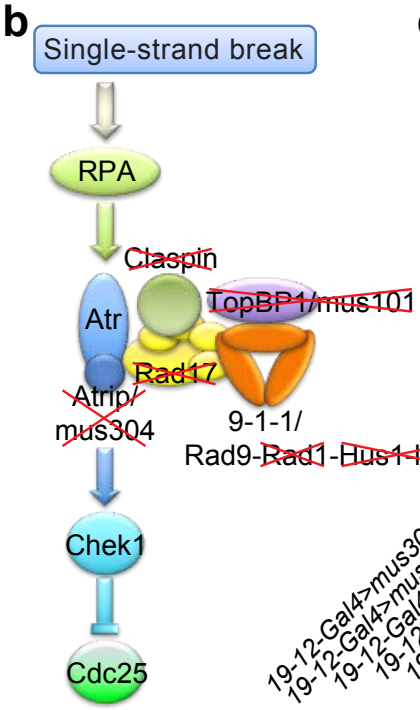

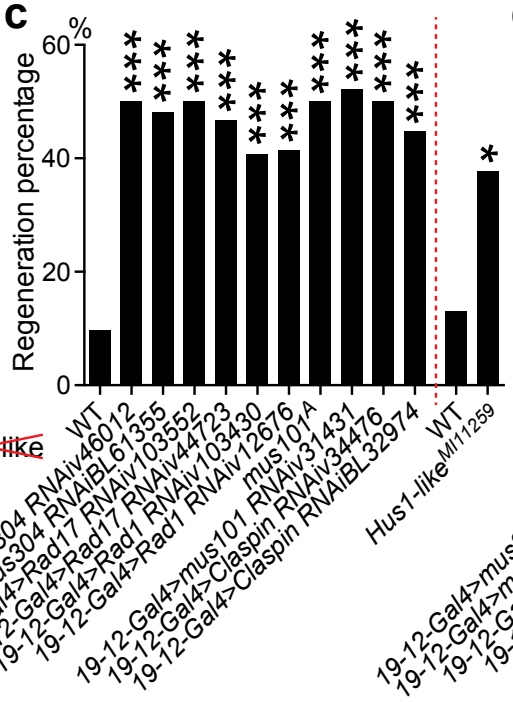

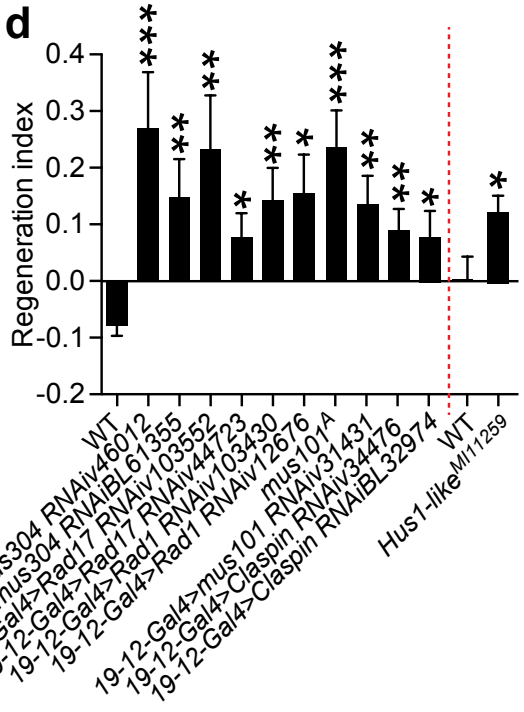

Figure 4

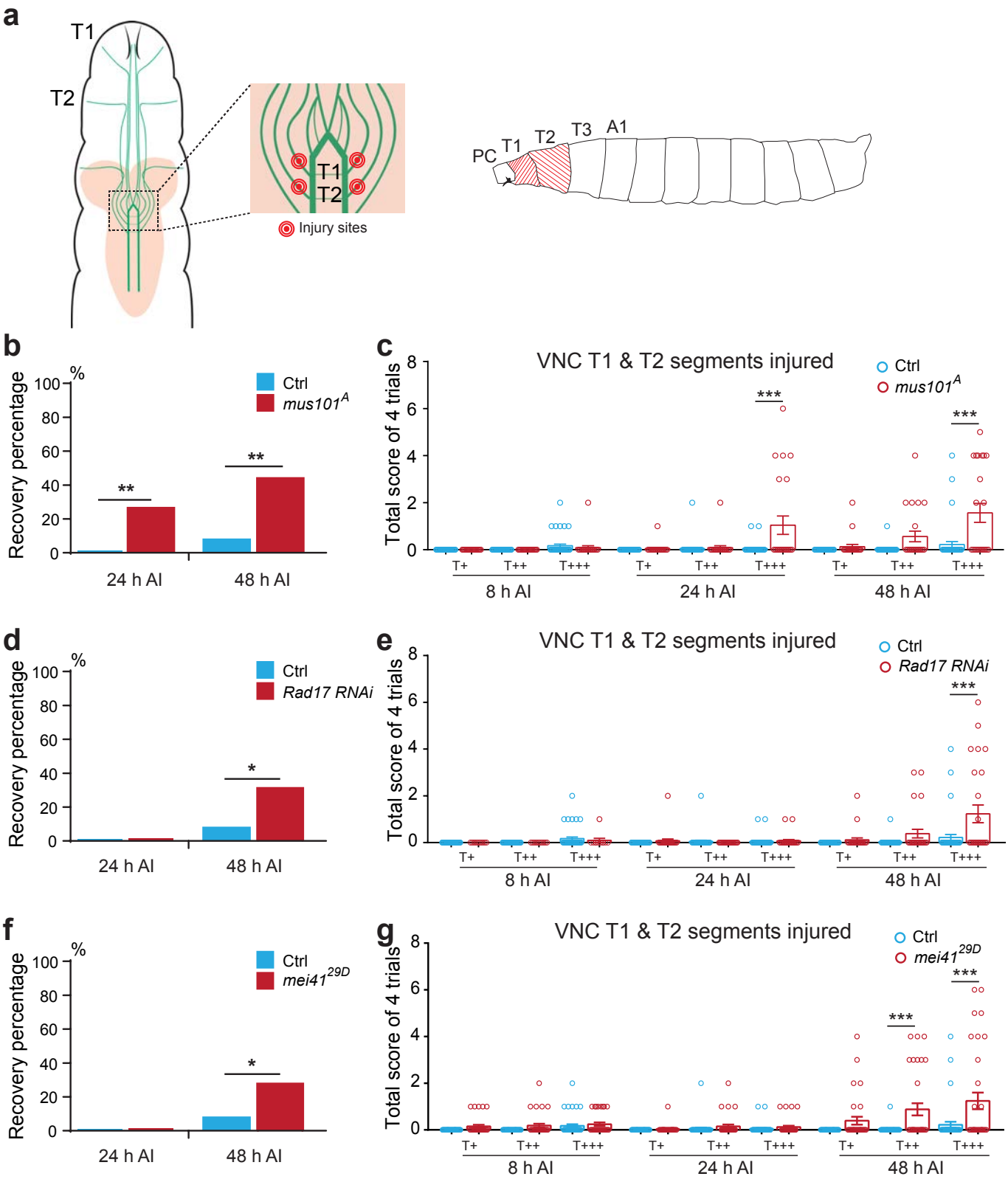

Figure 5

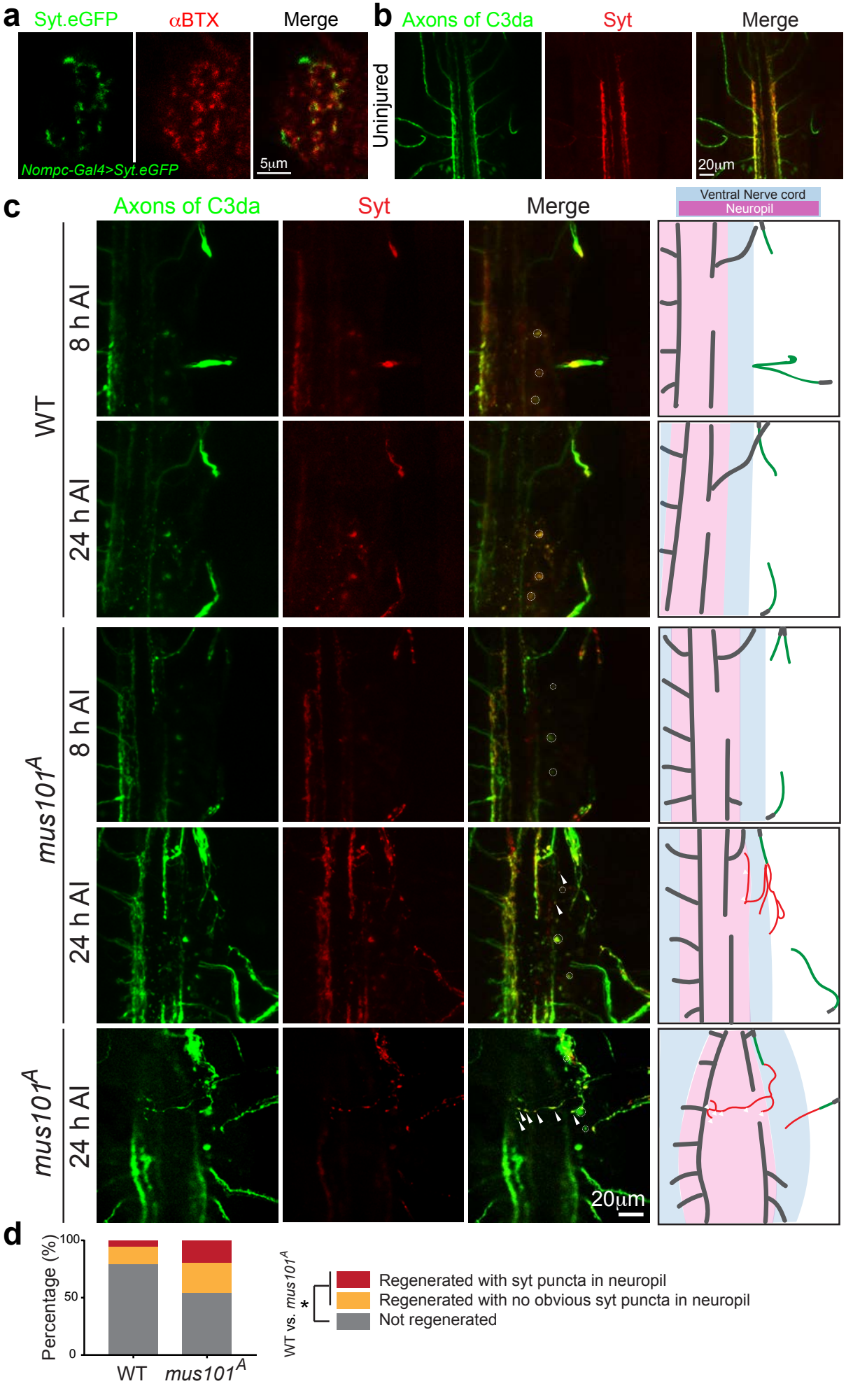

Figure 6

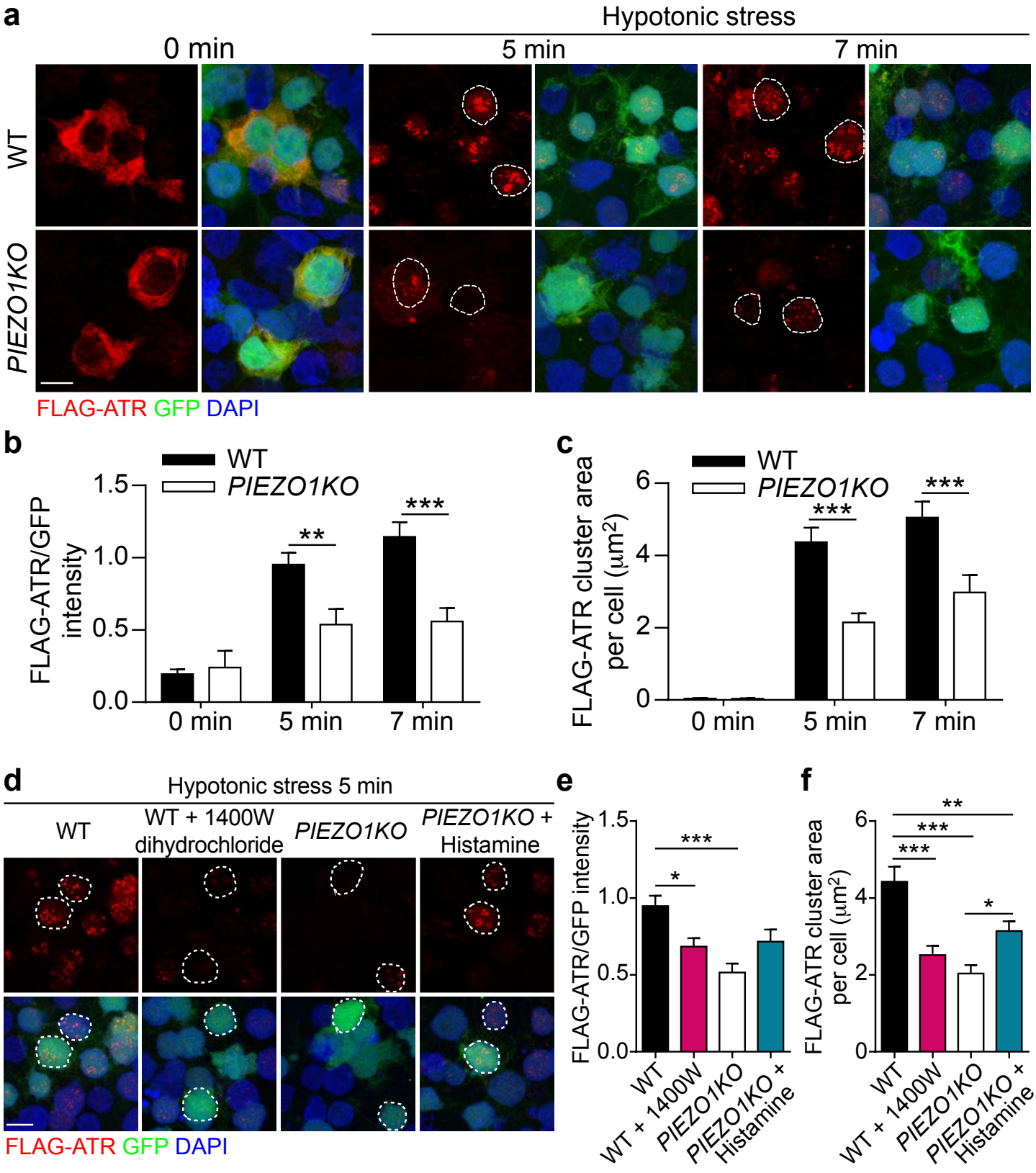

Figure 7

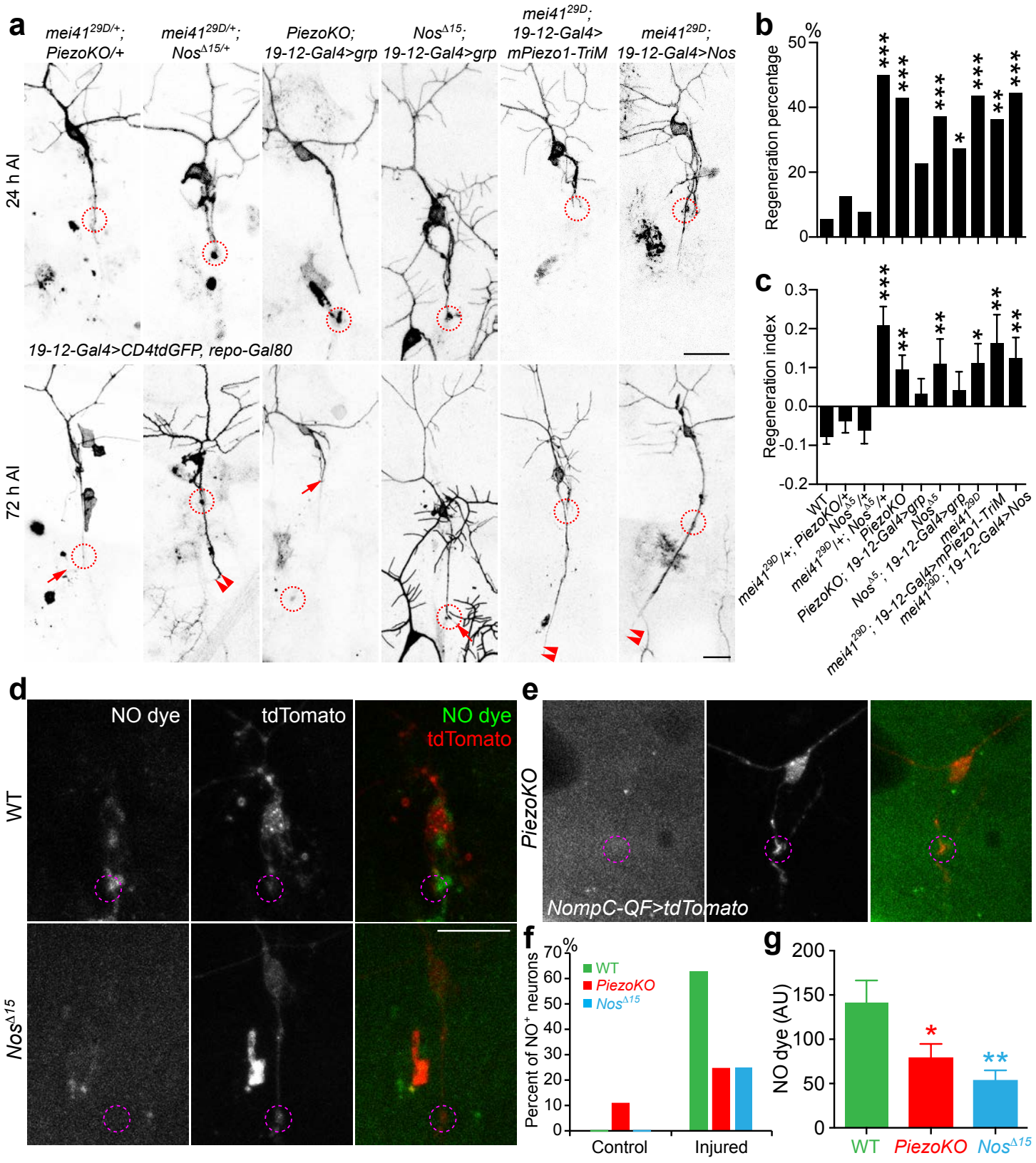

Figure 8

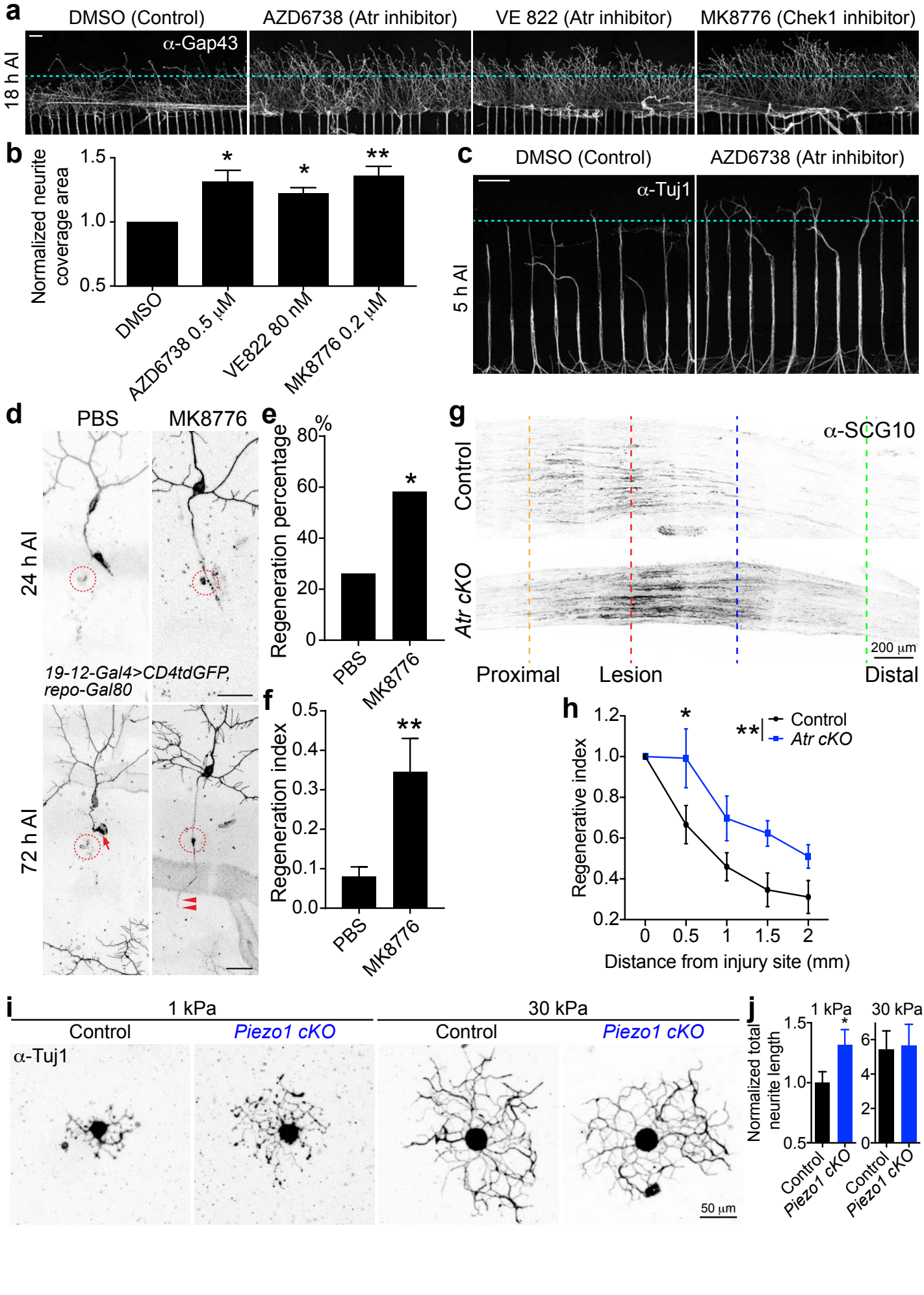

Supplementary Figure 1

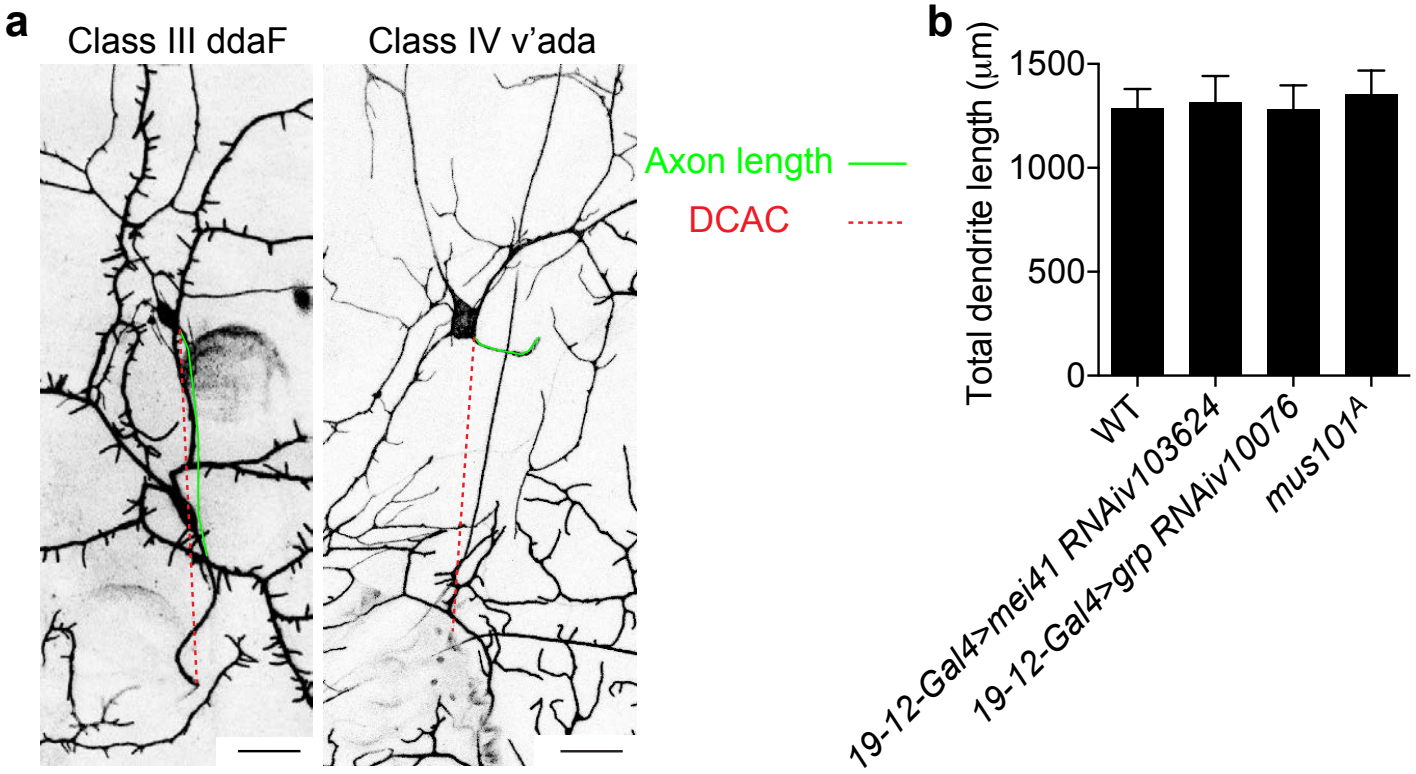

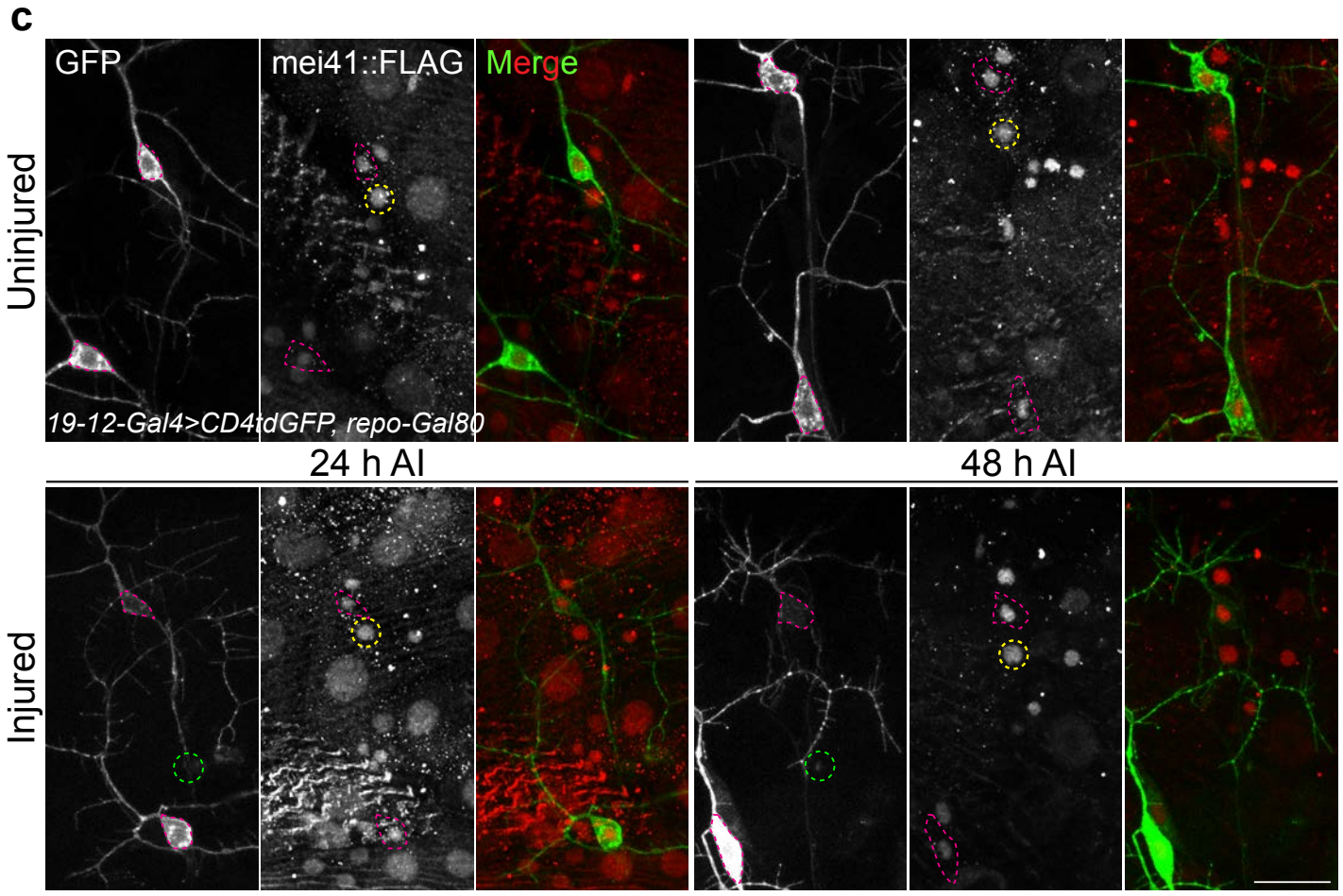

Supplementary Figure 2

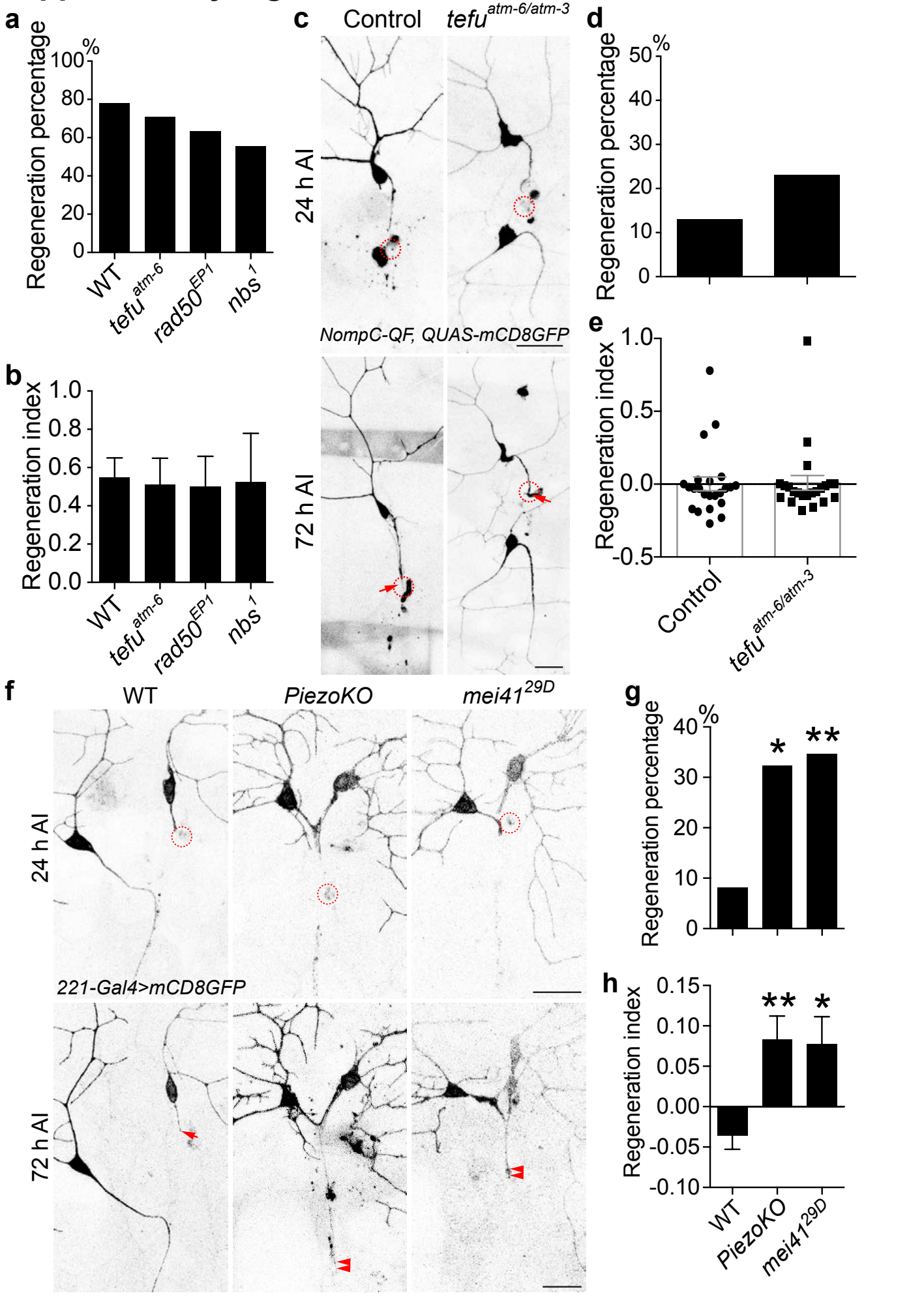

Supplementary Figure 3

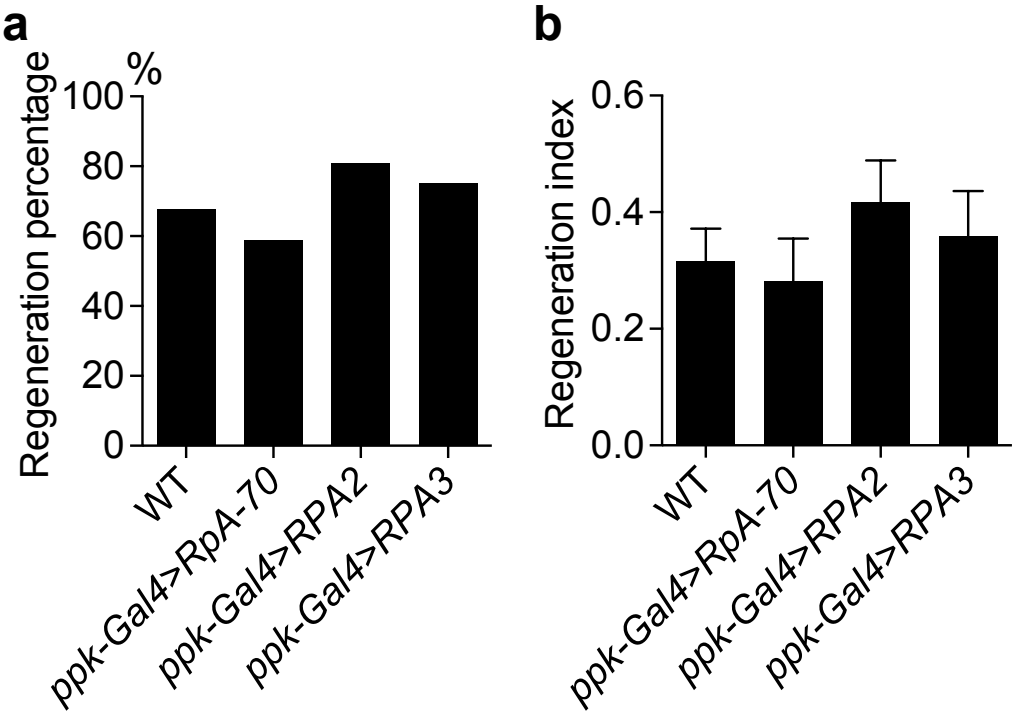

Supplementary Figure 4

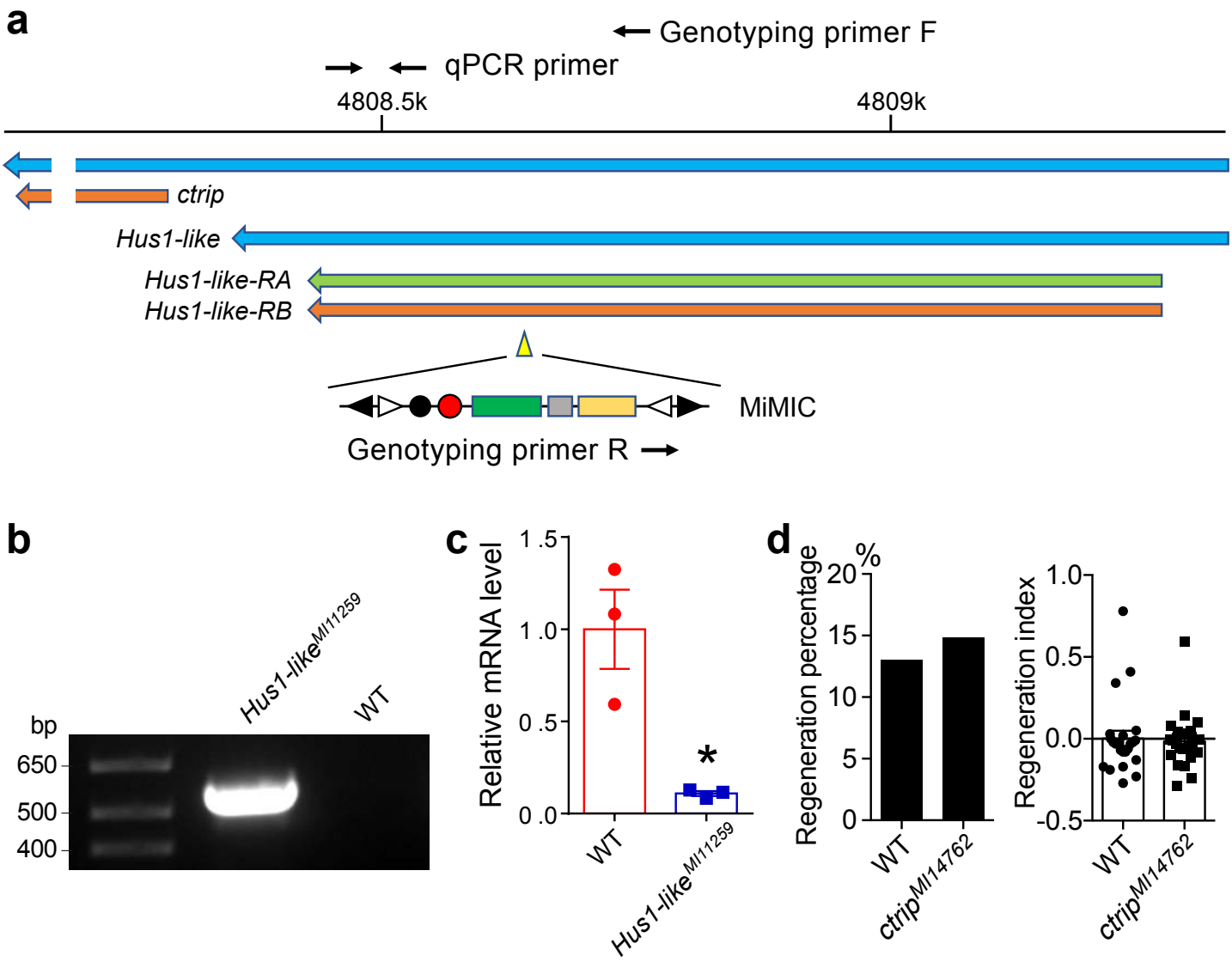

Supplementary Figure 5

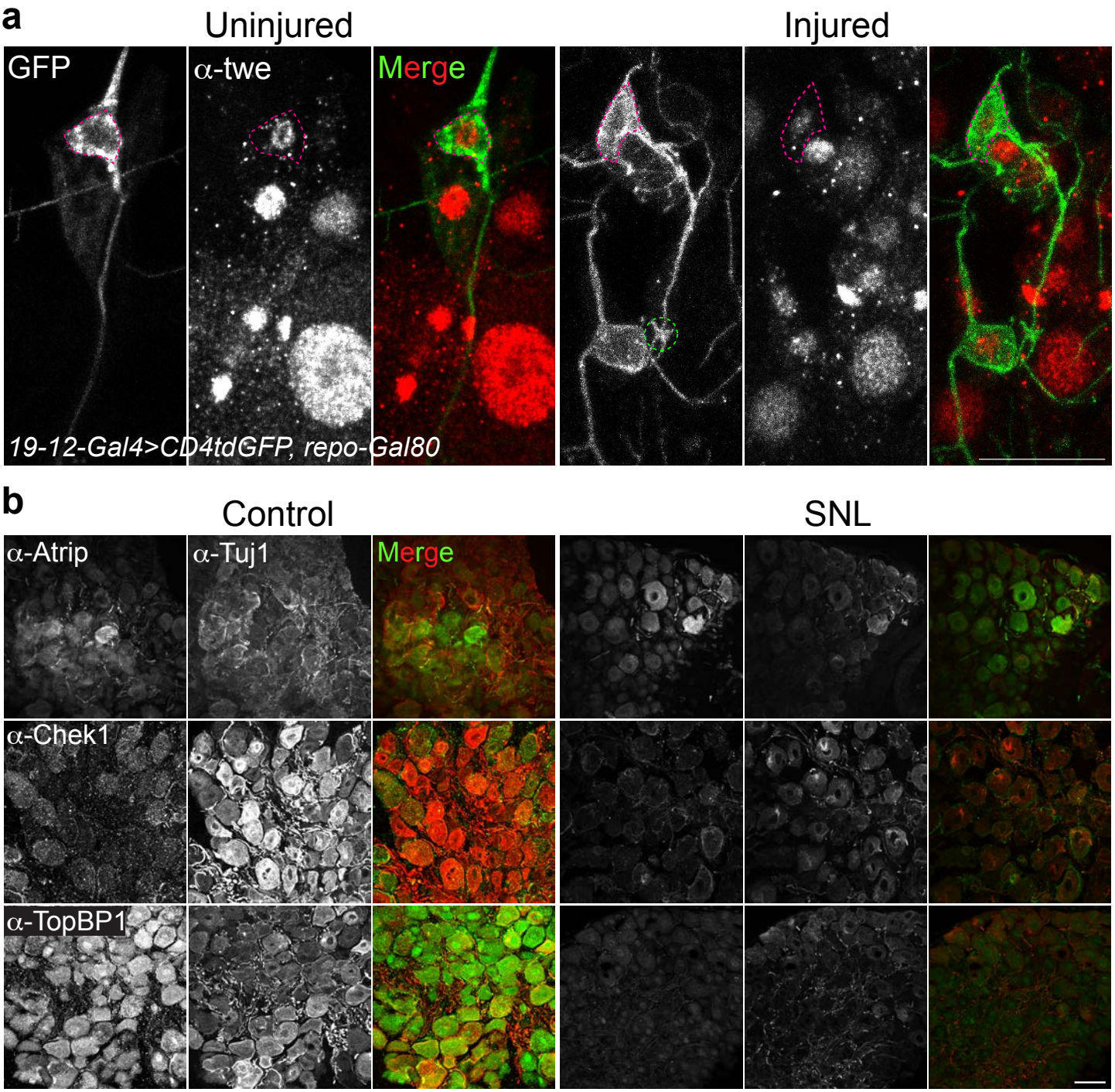

Supplementary Figure 6

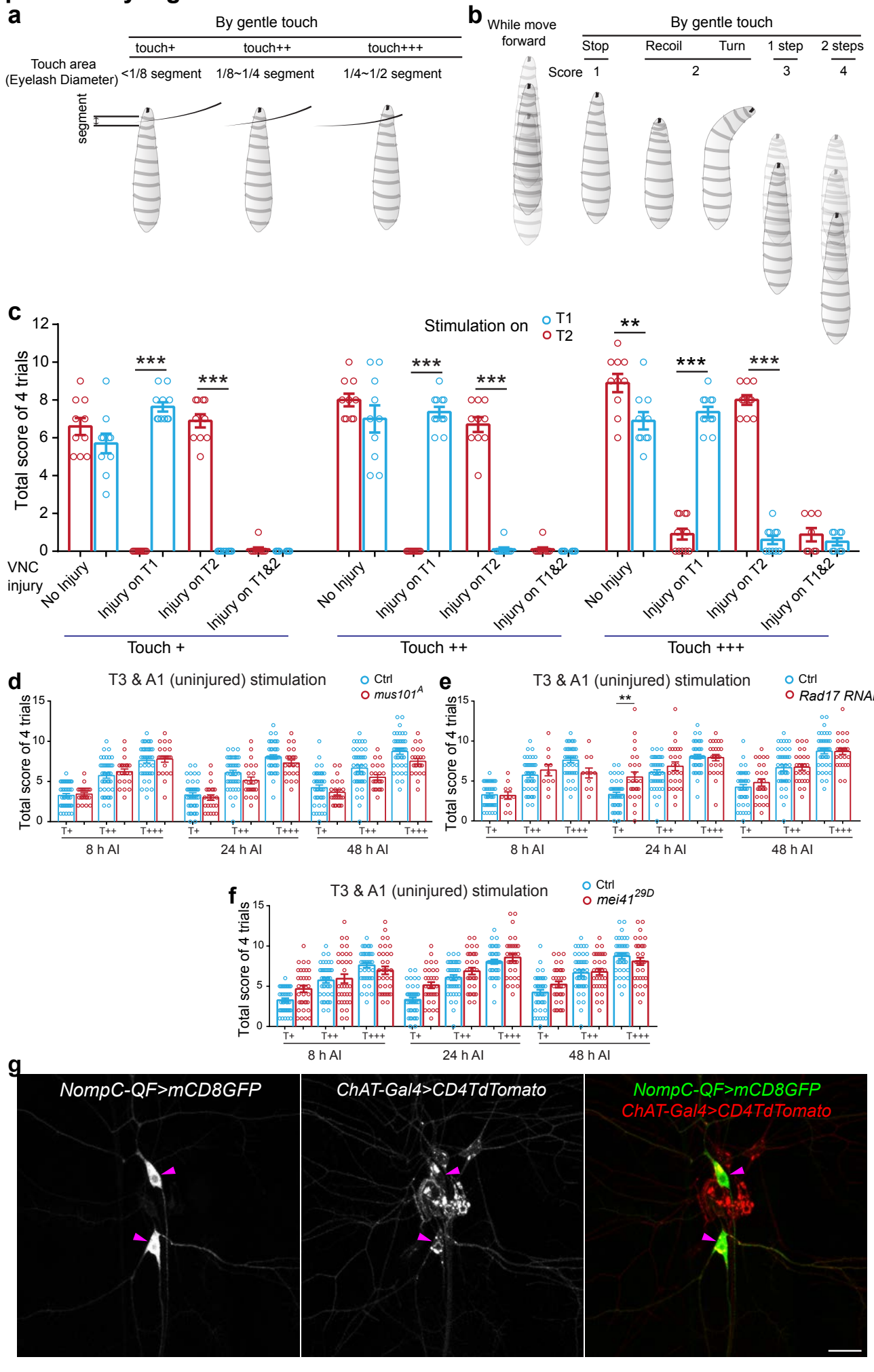

Supplementary Figure 7

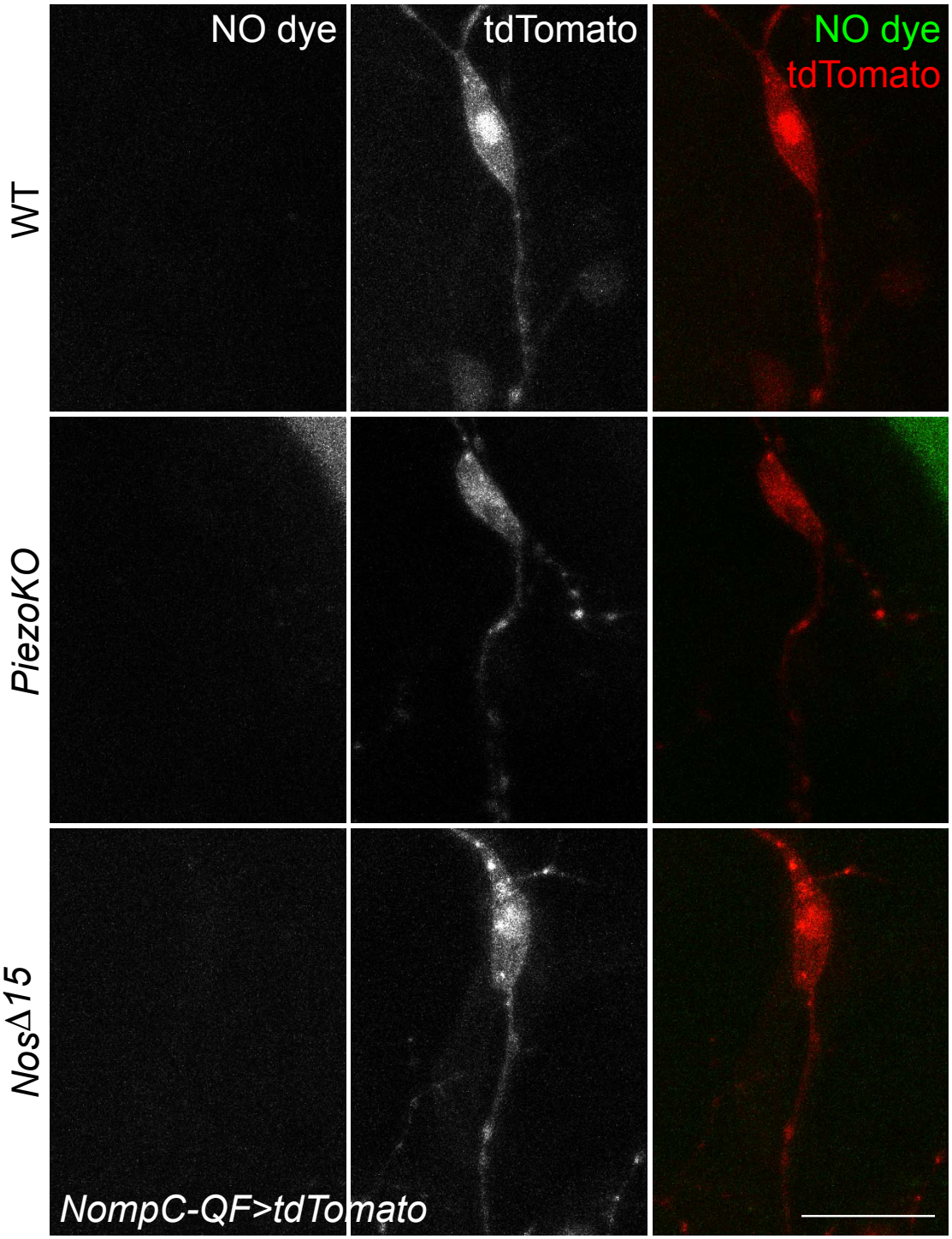

Supplementary Figure 8